$$P_b = \frac{1}{2} e^{-E_b/2N_0}, \tag{3.8.18}$$

and thus the curves shown in Figure 3.8.10 are produced.

Insight into the degradation for multihop noncoherent combining can be obtained from study of the decision p.d.f.'s. Figures 3.8.11a and 3.8.11b show decision p.d.f.'s for two cases with $E_b/N_0 = 10$ dB, the first with $H = 1$, that is, standard noncoherent detection of binary signals, and the second with $H = 5$. Obviously, the error probability suffers in the latter case, despite the fact that the total energy is equivalent. This is described as an inability to *coherently* integrate the available energy in a decision.

For M-ary orthogonal signaling with noncoherent detection, similar analysis pertains: one of the decision variables is noncentral chi squared with $2H$ degrees of freedom, while the remaining $M - 1$ variables are chi squared with $2H$ degrees of freedom. Proakis [31] formulates the exact expression for error probability in this case, leaving the result in integral form. A quick approximation uses the union bound for M-ary signaling:

$$P_s \leq (M - 1)P_b, \tag{3.8.19}$$

where P_b was expressed in (3.8.18) after correction for noncoherent combining loss.

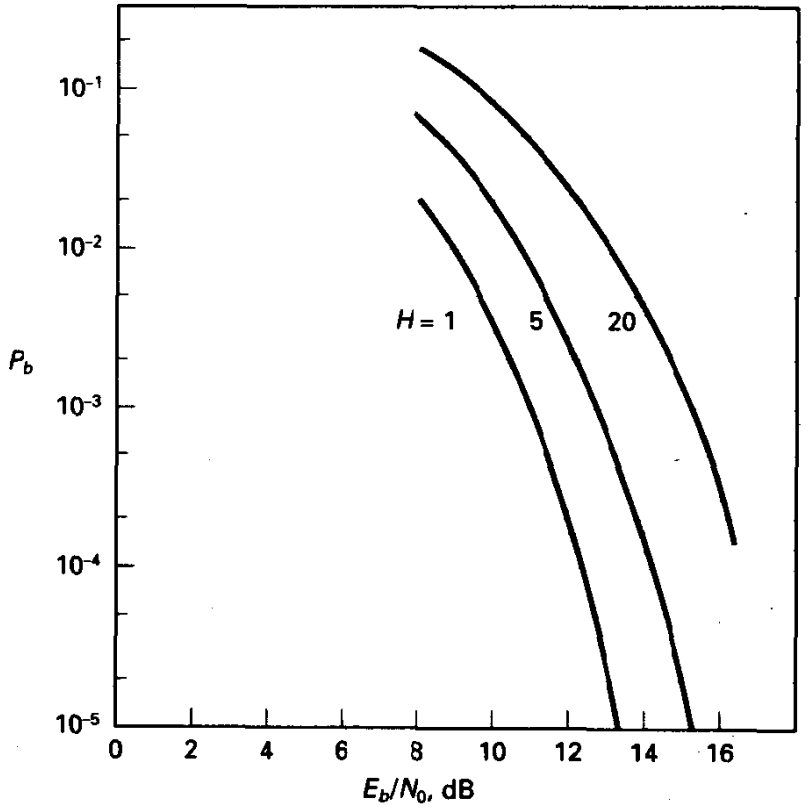

Figure 3.8.10 Error probability for frequency-hopping, binary orthogonal signals, H hops per bit.

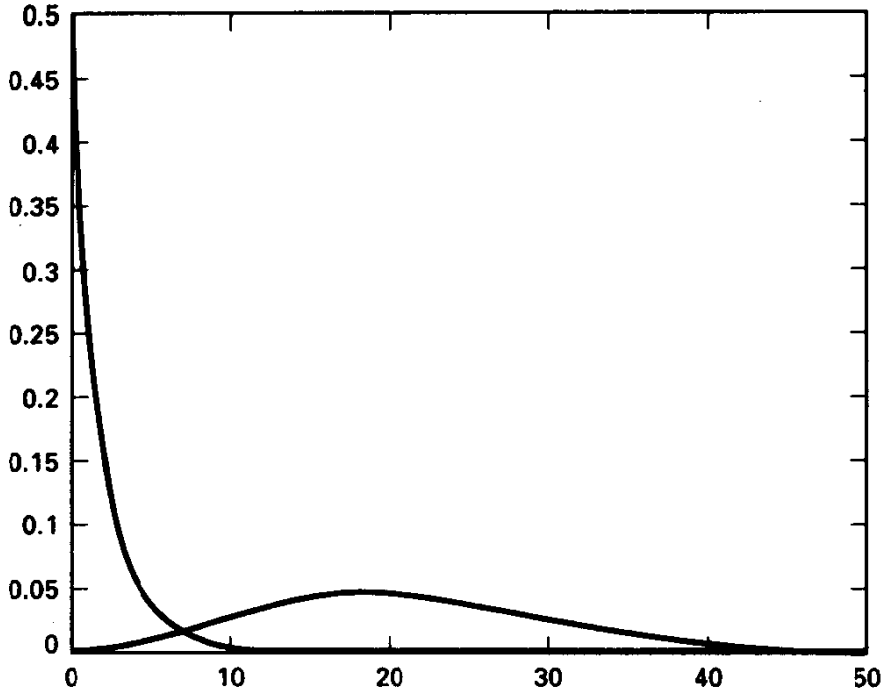

Figure 3.8.11a Decision variable p.d.f.'s for $H = 1$, $E_b/N_0 = 10$ dB.

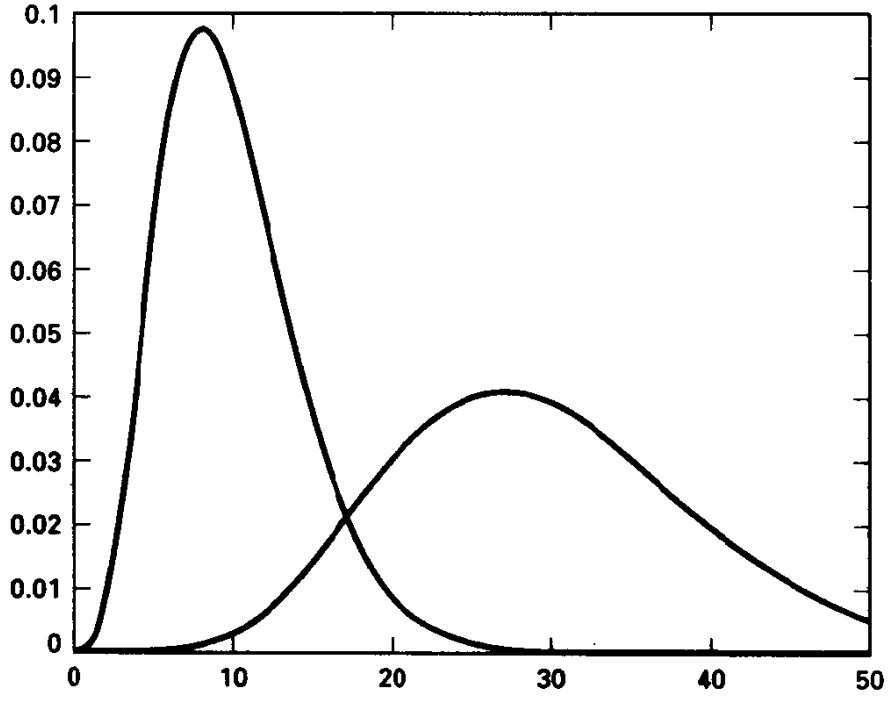

Figure 3.8.11b Decision variable p.d.f.'s for $H = 5$, $E_b/N_0 = 10$ dB.

Partial-band Interference in FH Systems

In the context of jamming environments, the question of worst-case jamming strategy arises. Specifically, given a set of resources (energy, bandwidth, and interferer power), we may ask about the worst-case jammer scenario and for the corresponding error probability. In FH systems, a ***partial-band jammer***, optimally configured, presents a difficult situation.

Consider first the case of *slow frequency hopping* over a total bandwidth of W hertz. Let us assume the jammer elects to broadcast a Gaussian noiselike signal having *total* power N_J at the intended receiver. The choice of a Gaussian jammer process is motivated by information-theoretic considerations—under a power constraint, additive Gaussian corruptions minimize channel capacity. If the noise were uniformly distributed in frequency across the entire band, the equivalent noise power density would be N_J/W W/Hz. Instead, let the jammer allocate this noise over some fraction ρ, called the ***fill factor***, of the entire bandwidth.[36] Once this fraction is specified, we assume that the interference spectrum is also hopped in frequency; otherwise, a smart transmitter could determine the location of the noise-free region and communicate freely.

In a region where interference exists, the power spectral density is

$$N_{0_J} = \frac{N_J}{\rho W} = \frac{N_0}{\rho} \tag{3.8.20}$$

where N_0 represents an average jammer noise density. In spectral regions where the interference is absent, we assume for simplicity that the receiver noise level is zero, and thereby perfect transmission is possible. On the other hand, in the case we hop onto a jammed region, referred to as a noise *hit*, we assume the performance is that of an AWGN channel with effective noise level N_{0_J}. The probabilities of these two events are $1-\rho$ and ρ, respectively. Hence the symbol error probability is

$$P_s(\rho) = \rho P[\text{error}|\text{noise level } N_{0_J}]. \tag{3.8.21}$$

This error probability depends on ρ and the problem resources, as well as the modulation and detection format. In principle, we may solve for the worst-case ρ that maximizes (3.8.21) and then the worst-case error probability. We will illustrate the process for the case of binary DPSK modulation.

Example 3.21 Worst-case Partial-band Interferer for Binary DPSK

For binary DPSK with noncoherent detection, (3.8.21) becomes

$$P_s(\rho) = \frac{\rho}{2} e^{-\rho E_b/N_0}. \tag{3.8.22}$$

Differentiating with respect to ρ and equating to zero yields the stationary point

$$\rho^* = \begin{cases} 1, & \dfrac{E_b}{N_0} < 1, \\ \left(\dfrac{E_b}{N_0}\right)^{-1}, & \dfrac{E_b}{N_0} \geq 1. \end{cases} \tag{3.8.23}$$

(Observe it makes no sense to have $\rho > 1$.) Equation (3.8.23) reveals that, for small ratios of signal energy to effective jammer noise level, the full-band strategy is most deleterious,

[36] We assume that the jammer knows all the parameters of our system, except the exact hopping pattern.

while as the jamming resources diminish, the best strategy is one that places noise in a decreasingly small fraction of the band. Again this only holds if the noise spectrum is continually reassigned in frequency so that a smart transmitter/receiver cannot dodge the interference.

Of equal interest is the corresponding error probability with ρ^* in effect. Substituting in (3.8.22) gives

$$P_s(\rho^*) = \begin{cases} \frac{1}{2}e^{-E_b/N_0}, & \frac{E_b}{N_0} < 1, \\ \frac{e^{-1}}{2E_b/N_0}, & \frac{E_b}{N_0} \geq 1. \end{cases} \tag{3.8.24}$$

In the second condition, the high SNR case, we find the particularly discouraging result that for worst-case partial-band noise the improvement in error probability is only an inverse dependence on E_b/N_{0_j}, rather than negative exponential. (This result assumes pessimistically that as E_b/N_{0_j} changes the optimal fill factor ρ is employed.) Figure 3.8.12 illustrates the error performance given in (3.8.24), showing the two regions specified in (3.8.24).

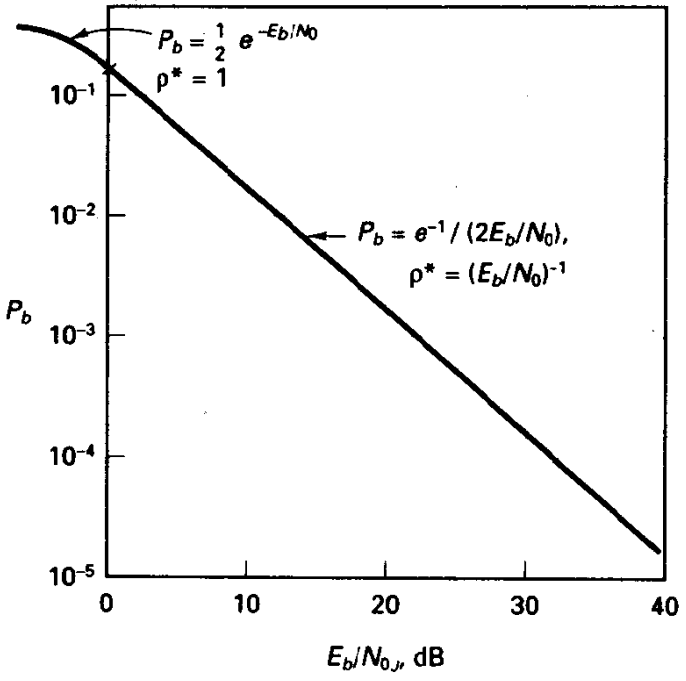

Figure 3.8.12 Error probability for worst-case partial-band noise; binary DPSK signals, slow frequency hopping, noncoherent detection.

Equation (3.8.24) also reveals that for a fixed jammer power N_J there is advantage to be gained with large hopping range W, since the jammer's effective signal-to-noise ratio E_b/N_0 is lowered. Herein we see the bandwidth-spreading advantage seen earlier for DS systems.

Similar results are obtained for all uncoded modulation formats, for example, MFSK and coherently detected MPSK. That is, the slope of the P_s curve plotted against E_b/N_0 is -1 for large arguments. We remark that this situation is also the case on the Rayleigh fading channel, where the resources are average signal energy and fixed noise level. It should be realized that the partial-band model breaks down in the case of

diminishing ρ^*. Specifically, if W is fixed, we eventually reach the situation where the optimal noise distribution is not a white noise process over the bandwidth of the received signal. In such cases, the interference approaches the tone-jammer model.

As with the fading channel, we will find that partial-band noise interference can be effectively mitigated by coding. Through channel coding, we may ensure that several noise hits are required to cause a decoding error. This has the effect of forcing the worst-case ρ to a larger value (to increase the hit probability) and changes the slope of the curve to a larger value. A particularly simple form of coding[37] that is effective against partial-band interference is represented by fast hopping—in essence, we encode the same message bit on H consecutive hops and model the encounter with interference as a Bernoulli trials experiment. If we assume that the receiver somehow can learn whether a given hop is noisy due to interference, the proper decision maker will never err unless *all* hops are jammed. This follows from the perfect trust in nonjammed hops, embodied through (3.8.14) or (3.8.15) when $\sigma^2 = 0$. The probability that all H hops encounter noise is ρ^H, and the probability of error becomes an extension of (3.8.21):

$$P_s(\rho) = \rho^H P(\text{error with } H \text{ hop combining}|\text{noise level } N_{0_j}). \tag{3.8.25}$$

This leads to the calculation of a worst-case ρ as before, and for $H > 1$, ρ^* is forced to a larger value (so that more hops will be hit on average), and the slope of the error probability curve versus E_b/N_{0_j} for large arguments is $-H$. Exercises 3.8.5 and 3.8.6 develop this result, as well as a related result pertaining to decisions on individual hops followed by majority voting. It is also worth noting that the fast-hopping strategy suffered against additive white Gaussian noise, relative to slow hopping, but against other impairment scenarios, fast hopping is perfectly sensible.

APPENDIX 3A1: ASYMPTOTIC PERFORMANCE OF *M*-ARY ORTHOGONAL SIGNALS

In Section 3.3 we observed that as M becomes large the symbol error probability for M-ary orthogonal signaling steadily decreased, at least for suitably large E_b/N_0. In Exercise 3.3.9 we show with a simple union bound that, provided $E_b/N_0 > 1.4$ dB, arbitrarily small error probability is obtained as $M \to \infty$. This is precisely 3 dB short of the channel capacity limit for the AWGN channel, and we here use a finer bounding technique to show that orthogonal signaling can, in fact, achieve the capacity limit. The treatment follows that of Viterbi and Omura [51], and the general procedure will be seen again in Chapter 4, where the performance of coded transmission on memoryless channels is studied.

We first assume that message S_0 is transmitted with no loss of generality due to signal and noise symmetry. The decision error region is expressed in terms of likelihood ratios:

$$D_0^c = \left\{ \mathbf{r} : \frac{f(\mathbf{r}|S_m)}{f(\mathbf{r}|S_0)} > 1 \text{ for some } m \neq 0 \right\}. \tag{3A1.1}$$

[37] This is known as repetition coding.

For $s > 0$, we can just as well express the error region as

$$D_0^c = \left\{\mathbf{r}: \left[\frac{f(\mathbf{r}|S_m)}{f(\mathbf{r}|S_0)}\right]^s > 1 \text{ for some } m \neq 0\right\}, \qquad s > 0. \tag{3A1.2}$$

The symbol error probability is

$$P_s = P[\mathbf{r} \in D_0^c | S_0], \tag{3A1.3}$$

and we can upper-bound P_s by including more of observation space in D_0^c. Thus, we define $\tilde{D}_0^c$ by

$$\tilde{D}_0^c = \left\{\mathbf{r}: \sum_{m=1}^{M-1} \left[\frac{f(\mathbf{r}|S_m)}{f(\mathbf{r}|S_0)}\right]^s \geq 1\right\} \tag{3A1.4}$$

and claim that every $\mathbf{r}$ found in D_0^c lies also in $\tilde{D}_0^c$. So

$$P_s \leq \int_{\mathbf{r}\in\tilde{D}_0^c} f(\mathbf{r}|S_0)\, d\mathbf{r} = \int_{\text{all } \mathbf{r}} g(\mathbf{r}) f(\mathbf{r}|S_0)\, d\mathbf{r}, \tag{3A1.5}$$

where $g(\mathbf{r}) = 1$ if $\mathbf{r} \in \tilde{D}_0^c$, and zero otherwise. The indicator, or step, function $g(\mathbf{r})$ is either 0 or 1 and can be upper-bounded, for $\rho > 0$, by

$$g(\mathbf{r}) \leq \left\{\sum_{m=1}^{M-1} \left[\frac{f(\mathbf{r}|S_m)}{f(\mathbf{r}|S_0)}\right]^s\right\}^\rho, \qquad \rho > 0. \tag{3A1.6}$$

Substituting in (3A1.5), we obtain

$$P_s \leq \int f(\mathbf{r}|S_0)^{1-s\rho} \left[\sum_{m=1}^{M-1} [f(\mathbf{r}|S_m)]^s\right]^\rho d\mathbf{r}. \tag{3A1.7}$$

We wish to minimize this bound over valid choices of s and ρ, but it is at least acceptable to pick $s = 1/(1+\rho)$, for $\rho > 0$. This choice in (3A1.7) gives

$$P_s \leq \int f(\mathbf{r}|S_0)^{1/(1+\rho)} \left[\sum_{m=1}^{M-1} [f(\mathbf{r}|S_m)]^{(1/1+\rho)}\right]^\rho \cdot d\mathbf{r}. \tag{3A1.8}$$

Now recall that, conditioned upon transmission of S_0, the demodulator output variables are all Gaussian, independent, with variance $N_0/2$. All means are zero except that of r_0, which is $E_s^{1/2}$. After manipulating exponents, we can write

$$f(\mathbf{r}|S_m) = \frac{\exp[(-E_s + 2E_s^{1/2} r_m)/N_0] \exp[-\sum_{m=0}^{M-1} r_m^2/N_0]}{(\pi N_0)^{M/2}}. \tag{3A1.9}$$

Employing this in (3A1.8) and simplifying, we obtain

$$P_s \leq e^{-E_s/N_0} \int \cdots \int \prod_{k=0}^{M-1} \frac{e^{-r_k^2/N_0}}{(\pi N_0)^{1/2}} \exp\left[\frac{2E_s^{1/2} r_0}{N_0(1+\rho)}\right] \left\{\sum_{m=1}^{M-1} \exp\left[\frac{2E_s^{1/2} r_m}{N_0(1+\rho)}\right]\right\}^\rho d\mathbf{r}. \tag{3A1.10}$$

If we change variables using $z_n = r_n/(N_0/2)^{1/2}$, then

$$P_s \le e^{-E_s/N_0} \int \cdots \int \prod_{k=0}^{M-1} \frac{e^{-z_k^2/2}}{(2\pi)^{1/2}} t(z_0) \left[\sum_{n=1}^{M-1} t(z_n) \right]^{\rho} dz, \tag{3A1.11}$$

where $t(z_m) = \exp\left[\left(\frac{2E_s}{N_0} \right)^{1/2} \frac{z_m}{1+\rho} \right]$. We can now recognize (3A1.11) as an expectation with respect to r.v.'s $\{Z_k\}$, which are independent, zero-mean, unit-variance Gaussian variables. Independence gives

$$P_s \le e^{-E_s/N_0} E[t(z_0)] E\left[\left(\sum_{n=1}^{M-1} t(z_n) \right)^{\rho} \right]. \tag{3A1.12}$$

The definition of expectation and completion of the square yield the first expectation:

$$E[t(z_0)] = \exp\left[\frac{E_s}{N_0(1+\rho)^2} \right]. \tag{3A1.13}$$

For the second expectation in (3A1.12), we use Jensen's inequality (see Exercise 2.3.7). Let's define the r.v. $Y = \sum_{n=1}^{M-1} t(Z_n)$, which can be seen to be nonnegative. We seek then $E[Y^{\rho}]$, which by Jensen's inequality is bounded by

$$E[Y^{\rho}] \le \{E[Y]\}^{\rho}, \qquad 0 \le \rho \le 1. \tag{3A1.14}$$

(Note that raising a number to a fractional power constitutes a convex $\cap$ functional transformation.) Thus,

$$\begin{aligned} E[Y^{\rho}] &\le \left\{ E\left[\sum_{n=1}^{M-1} t(Z_n) \right] \right\}^{\rho} = \{(M-1)E[t(Z_1)]\}^{\rho} \\ &= (M-1)^{\rho} \exp\left[\frac{E_s \rho}{N_0(1+\rho)} \right]. \end{aligned} \tag{3A1.15}$$

By using $M - 1 < M$,

$$\begin{aligned} P_s &\le M^{\rho} e^{-E_s/N_0} e^{E_s/[N_0(1+\rho)]} \\ &< M^{\rho} \exp\left[-\frac{E_s}{N_0} \left(\frac{\rho}{1+\rho} \right) \right], \qquad 0 \le \rho \le 1. \end{aligned} \tag{3A1.16}$$

Now we recall that $E_s = E_b \log_2 M$ and proceed to minimize the bound through choice of ρ. Doing so by standard calculus reveals that the best ρ is

$$\rho^* = \left[\frac{E_b}{N_0 \log_e 2} \right]^{1/2} - 1, \tag{3A1.17}$$

which will lie in the interval [0, 1) as required by the bounding procedure, provided that $\log_e 2 < E_b/N_0 < 4 \log_e 2$. (For larger E_b/N_0 values, we simply use $\rho = 1$ as the maximizing ρ; in fact, for such cases this procedure is equivalent to that developed in Exercise 3.3.9.) Back-substitution of ρ^* into (3A1.16) yields

$$P_s \le e^{-\log_2 M \left(\frac{E_b}{N_0} + 1 \right)}, \qquad \log_e 2 < \frac{E_b}{N_0} < 4 \log_e 2. \tag{3A1.18}$$

This demonstrates then that, provided $E_b/N_0 > \log_e 2 = 0.693 = -1.6$ dB, use of orthogonal signals with $M \to \infty$ gives arbitrarily small error probability. We will not develop the *strong converse*, that when $E_b/N_0 < \log_e 2$ as $M \to \infty$, P_s approaches 1.

APPENDIX 3A2: LATTICES

A lattice is a set of points in N-dimensional Euclidean space arranged in highly regular manner. In the digital communication context, a lattice may serve as a constellation, by truncating the lattice to a finite set of M smallest-energy points nearest the origin, or the lattice may serve as a framework for coded transmission by partitioning the lattice into smaller disjoint sublattices and then applying block or trellis coding constructions to map information sequences onto a sequence of subsets. Moreover, the theory of lattices can provide interesting generalizations of more traditional coding approaches involving binary block codes, as described in Chapter 5.

Our discussion follows the presentation of Forney [52], and notation is that of the standard literature on lattices. The text by Conway and Sloane [53] is considered the encyclopedia on this subject. We will begin with some familiar lattices that are easily visualized.

Some Familiar Examples

The simplest lattice, and the only one-dimensional lattice, is designated $\mathbf{Z}$, the set of integers (see Figure 3A2.1). Each lattice point is adjacent to two others, and the closest lattice point is one unit distant. In two dimensions, the set of points with integer-valued coordinates is denoted as $\mathbf{Z} \times \mathbf{Z} = \mathbf{Z}^2$, but a slightly better arrangement of lattice points, for digital communication purposes, derives from the ***hexagonal lattice***, $\mathbf{A}_2$, a portion of which is shown in Figure 3A2.2. (The name hexagonal refers to the nearest-neighbor decision zones surrounding each lattice point.) Here the number of adjacent lattice points is 6, but the minimum Euclidean distance between points remains at 1, despite the increase in the number of points per unit area. In three dimensions, the ***face-centered-cubic (fcc) lattice***, shown in Figure 3A2.3, is known to provide the centers for the densest packing of spheres, or balls, and this lattice is designated $\mathbf{D}_3$. Notice that all lattice points have integer-valued coordinates whose sum is even; this lattice forms a subset of the three-dimensional lattice $\mathbf{Z}^3$.

These examples have much common structure. First, the sets of points form a group under ordinary addition of N-tuples. That is, the addition of any two points in

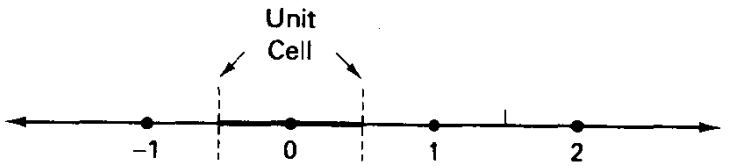

Figure 3A2.1 Lattice $\mathbf{Z}$, $d_{\min} = 1$.

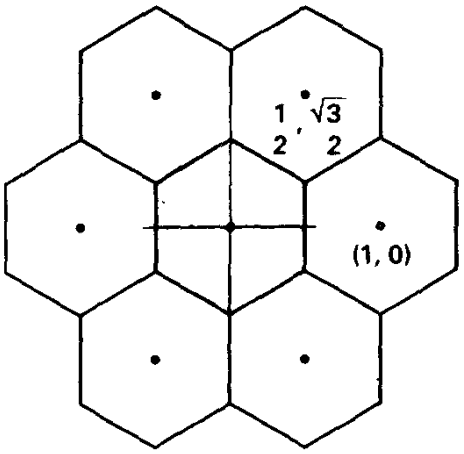

Figure 3A2.2 Lattice A_2, $d_{\min} = 1$.

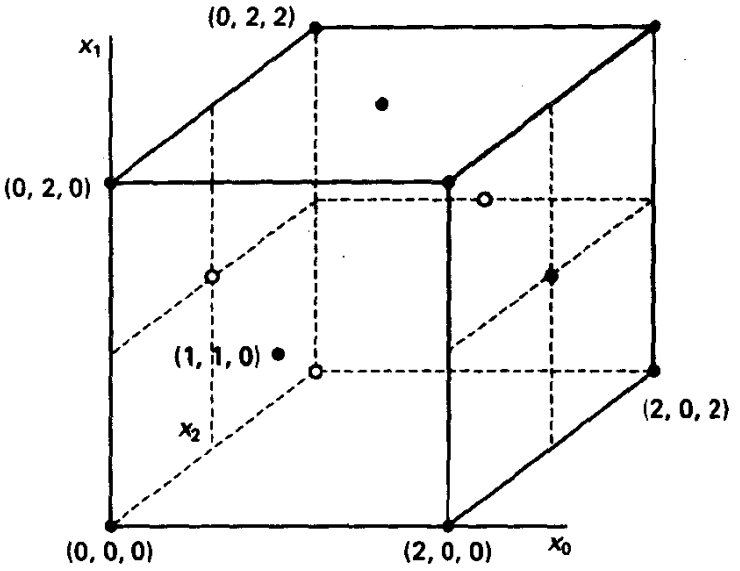

Figure 3A2.3 D_3 lattice points (face-centered cubic lattice).

the lattice produces another. Equivalently, each lattice point is expressible as a sum of integer multiples of basis vectors. Furthermore, we notice extreme regularity—the lattice looks the same no matter on which point we stand. With some simple ideas in mind, we now formalize the algebraic and geometric structure of lattices and then proceed to describe higher-dimensional lattices. (The fact that we have difficulty visualizing higher-dimensional objects should not be a deterrent to their description or use.)

Algebraic and Geometric Notions about Lattices

A real ***lattice*** Λ is a countably infinite collection of points, or vectors, or N-tuples, in real Euclidean N-dimensional space that form an algebraic group under ordinary vector addition. We denote the points by vectors of the form $\mathbf{x} = (x_0, x_1, \ldots, x_{N-1})$, so x_i are

the Cartesian coordinates of a lattice point in N-space. Eventually, these points become the signal-space coordinates of a signal set.

The group property requires that the vector sum or difference of any two elements of the lattice be in the lattice and that the lattice include the point **0**. To say that the lattice is N-dimensional means that exactly N basis vectors, not necessarily orthogonal, are required to span the countable set. Thus, points of a lattice are described in terms of a $N \times N$ generator matrix **M** by

$$\mathbf{x} = \mathbf{uM}, \tag{3A2.1}$$

but where the components of the "message" **u** are *integer valued.* Thus, a lattice is the set of all linear combinations of integer multiples of the rows of **M**. For example, $\mathbf{A}_2$ has obvious basis vectors $(1, 0)$ and $(\frac{1}{2}, 3^{1/2})$; thus,

$$\mathbf{M} = \begin{bmatrix} 1 & 0 \\ \frac{1}{2} & \frac{3^{1/2}}{2} \end{bmatrix} : \mathbf{A}_2 \tag{3A2.2}$$

In four-dimensional space, the most useful lattice is the Schlafli lattice $\mathbf{D}_4$, defined by[38]

$$\mathbf{M} = \begin{bmatrix} 2 & 0 & 0 & 0 \\ 1 & 0 & 0 & 1 \\ 0 & 1 & 0 & 1 \\ 0 & 0 & 1 & 1 \end{bmatrix} : \mathbf{D}_4 \tag{3A2.3}$$

If $\mathbf{u} = (-1, 0, 2, 0)$, for example, the corresponding lattice point is $\mathbf{x} = (-2, 2, 0, 2)$.

Although the matrix formulation is a sufficient description, we often describe a lattice by specifying the constraints placed on its constituent points; for example, "$\mathbf{D}_4$ is the set of integer-valued 4-tuples whose sum of coordinates is even," as may be seen by study of **M** in (3A2.3). There is, of course, no unique matrix description for a lattice.

Certain operations on lattices leave the basic properties unchanged. ***Scaling*** of a lattice corresponds to stretching the coordinate system equally in all dimensions by multiplying **M** by a scalar a; the corresponding lattice will be designated $a\Lambda$. This will change the distance between points proportionately, but all other features of the lattice remain unaltered. ***Translation***, by adding an N-tuple **c** to all lattice points, produces the lattice designated $\Lambda + \mathbf{c}$. This is useful in minimizing the energy of a finite constellation drawn from a lattice. ***Rotation*** of a lattice produces a new lattice $\mathbf{O}\Lambda$ and is obtained by multiplying **M** by an orthogonal matrix **O**, that is, one for which $\mathbf{OO}^T = a\mathbf{I}$. If a lattice Λ_1 can be obtained from another lattice Λ by a series of scaling, translation, or rotation operations, we say that the two lattices are similar, or ***congruent***, and express this as $\Lambda_1 \sim \Lambda$. Finally, the Cartesian product lattice Λ^M is the set of MN-tuples $(\lambda_0, \lambda_1, \ldots, \lambda_{M-1})$, where each $\lambda_i \in \Lambda$. Thus, $\mathbf{Z}^N$, for example, is just the set of integer-valued N-tuples. (Note superscripts represent Cartesian products of lattices, while subscripts denote dimensions of lattices.)

Now for some geometric concepts attached to lattices. Most important is the minimum Euclidean distance between any pair of points in the lattice, $d_{\min}$. Because of the regularity of the lattice, $d_{\min}$ is invariant to choice of reference point. In $\mathbf{Z}^N$, $d_{\min} = 1$, and $d_{\min}$ in $\mathbf{A}_2$ is also 1. In $\mathbf{D}_4$ defined previously, the point $(0, 0, 0, 0)$ has a nearest lattice point with coordinates $(1, 1, 0, 0)$, and hence $d_{\min} = 2^{1/2}$.

[38]Other equivalent definitions are common.

Suppose we center N-dimensional spheres with radius $d_{\min}/2$ at each lattice point. These spheres will touch or "kiss" a finite number of similar spheres. This number is called the ***kissing number*** of the lattice, often denoted by τ. For $\mathbf{Z}^N$, the kissing number is $2N$; $\mathbf{A}_2$ has a kissing number 6. $\mathbf{D}_3$, the face-centered-cubic lattice, and $\mathbf{D}_4$ have kissing numbers 12 and 24, respectively. [In $\mathbf{D}_4$, the points nearest the origin are the 24 points of the form $(\pm 1^2, 0^2)$, denoting vectors with exactly two ± 1's and two 0's in four positions. Spheres around these points having radius $2^{1/2}$ all kiss the sphere centered at the origin.]

Each lattice point has a region surrounding it, called the nearest-neighbor zone, or more technically the ***Voronoi zone***,[39] which contains the region in $\mathbf{R}^N$ closer to the given lattice point than to any other and which constitutes decision zones for the Gaussian channel environment. The Voronoi region will be a polyhedron in N-space having a number of faces equal to the kissing number, since the Voronoi zones are bounded by planes bisecting lines connecting a point to its nearest neighbors. These polyhedra circumscribe the spheres of radius $d_{\min}/2$ around each point.

For $\mathbf{Z}^N$, the Voronoi region is an N-cube with unit edge length, while $\mathbf{A}_2$'s unit cell is a hexagon (hence the common name for this lattice). $\mathbf{D}_3$'s Voronoi cell is a dodecahedron, and $\mathbf{D}_4$ has a 24-faceted polyhedron in 4-space as the Voronoi region. Again because of the regularity of a lattice, the Voronoi regions surrounding each point are identical and form a disjoint partition of $\mathbf{R}^N$.

It will be important in assessing communication efficiency to determine the volume of the Voronoi cell for an arbitrary lattice Λ. It is known [53] that this volume is precisely

$$V(\Lambda) = \det \mathbf{M} \tag{3A2.4}$$

and thus, if we know the generator matrix, finding the volume $V(\Lambda)$ is easy. In particular, since $\mathbf{Z}^N$ has $\mathbf{M} = \mathbf{I}$, the volume of its unit cell is 1, consistent with knowledge that the cell is the N-cube with unit edge length. An alternative, and easier method to find $V(\Lambda)$ for general lattices will follow shortly based on lattice decompositions.

Owing to the group structure, a lattice may be decomposed into a sublattice (a subgroup) and its cosets. More specifically, a ***sublattice*** Λ' of a parent lattice Λ is another lattice that is a subset of Λ. In algebraic terms, we would say Λ' is a subgroup of Λ, and it induces a ***partition*** or decomposition of Λ into equivalence classes, formed by Λ' and its cosets, or translates. A ***coset*** of a lattice Λ' is simply the set of points $\lambda' + \mathbf{c}$, where $\lambda' \in \Lambda'$. The ***order*** of such a partition is the number of equivalence classes so formed. In set notation terms, we say

$$\Lambda = \Lambda' \cup (\Lambda' + \mathbf{c}_1) \cup \ldots \cup (\Lambda' + \mathbf{c}_B) \tag{3A2.5}$$

for a partition of order B.

Example 3A2.1 Partitioning the $\mathbf{Z}_2$ Lattice

As earlier noted, the lattice $\mathbf{Z}^2 = \mathbf{Z} \times \mathbf{Z}$ is the set of integer-valued coordinate pairs. This set may be divided into two disjoint sets defined by the points whose coordinate sum is 0, mod 2, and the set whose sum is 1, mod 2. Thus, the point $(0, 0)$ is in the first set, while $(2, 3)$ is in the second set. This partitioning defines two closely related sublattices,

[39] Also called the unit cell.

one being the set of points (x_0, x_1) for which

$$x_0 + x_1 = 0, \qquad \text{mod } 0, \tag{3A2.6}$$

and the second obtained by adding the coordinate pair $(1, 0)$ to every point of the first set.

The partitioning can be easily visualized by imagining a checkerboard of red and black squares. The original lattice consists of points at the center of every square. The two sublattices are merely the center points of the red and black squares, respectively. You should observe that the two cosets so obtained are fundamentally identical in nature, having the same number of nearest neighbors, same distance structure between points, and so on. It is also important to observe that the minimum intraset distance between points of a set increases by $2^{1/2}$ when we subdivide here, for points formerly nearest neighbors in the original lattice are no longer members of the same set.

The points with zero sum, mod 2, form the sublattice called $\mathbf{D}_2$, and so we can write the decomposition simply as $\mathbf{Z}^2 = \mathbf{D}_2 \cup [\mathbf{D}_2 + (1, 0)]$. However, notice from the checkerboard representation that $\mathbf{D}_2 \sim \mathbf{Z}^2$, since these points can be seen to be a rotated (by 45°) and scaled (by $2^{1/2}$) version of $\mathbf{Z}^2$.

The lattice partitioning can be continued indefinitely, assuming an arbitrarily big initial set, each time producing sublattices again. For example, subdivision of $\mathbf{D}_2$ produces two copies of $2\mathbf{Z}^2$ within which the minimum distance is now 2. A ***partition chain*** is a sequence of lattices $\Lambda, \Lambda', \Lambda'', \ldots$, for which each successive lattice is a sublattice of the former. We express such chains as $\Lambda/\Lambda'/\Lambda'', \ldots$. For the preceding example, an indefinite partition chain of the form $\mathbf{Z}^2/\mathbf{D}_2/2\mathbf{Z}^2/2\mathbf{D}_2/ \ldots$ results. We could skip intermediate partitions in the sequence and observe that $\mathbf{Z}^2/2\mathbf{Z}^2$ is a partition of order 4.

Most of the important lattices are ***integer lattices***, ones for which all coordinates are integers (note $\mathbf{A}_2$ is not one), and it is usually the case that $2^m\mathbf{Z}$ will be a sublattice of an N-dimensional lattice Λ for some m. If so, Λ is a ***binary lattice***. If $m = 1$, Λ is a mod-2 binary lattice; if $m = 2$, it is called a mod-4 binary lattice. $\mathbf{D}_2$ is a mod-2 binary lattice, as is the following example.

Example 3A2.2 $\mathbf{D}_4$ Partition Chain

$\mathbf{D}_4$ is an order-2 partition of $\mathbf{Z}^4$, since one definition is the set of all integer 4-tuples whose sum is even. $\mathbf{D}_4$ may be further subdivided into $R\mathbf{D}_4$ (and three cosets), where R is the two-dimensional rotation operator

$$R = \begin{bmatrix} 1 & 1 \\ 1 & -1 \end{bmatrix} \tag{3A2.7}$$

and we interpret the lattice $R\Lambda$ to mean the lattice to which the rotation operator is applied to pairs of coordinates separately. In this notation, the lattice operator R^2 is equivalent to multiplication by $2\mathbf{I}$, or scaling the lattice by 2. To illustrate, $R\mathbf{D}_4$ is the set of integer 4-tuples whose total sum is even and whose first and last coordinate pairs sum to an even number. In this lattice, $d_{\min} = 2$ still. It can be seen that *four* translates of $R\mathbf{D}_4$ form $\mathbf{D}_4$. Going one step further, we can subdivide $R\mathbf{D}_4$ into two copies of $2\mathbf{Z}^4$, within which $d_{\min} = 2$. Thus, $\mathbf{Z}^4/\mathbf{D}_4/R\mathbf{D}_4/2\mathbf{Z}^4$ represents a partition chain whose total order is 16 and whose profile of $d^2_{\min}$ is 1/2/2/4.

If we adopt a single point in each coset of a partition Λ/Λ' as a ***coset representative***, we obtain a system of coset representatives, designated by $[\Lambda/\Lambda']$, whose number is the order of the partition. In the previous example, coset representatives for the two-way

partition $\mathbf{Z}^2/\mathbf{D}_2$ could be taken as $(0, 0)$ and $(1, 0)$. In the four-way partition $\mathbf{D}_4/R\mathbf{D}_4$, the coset representatives could be $(0, 0, 0, 0)$, $(0, 1, 0, 1)$, $(1, 0, 1, 0)$, and $(1, 0, 0, 1)$, since any of these vectors, when added to any point in $R\mathbf{D}_4$, is in $\mathbf{D}_4$.

Such a progressive decomposition provides a means of defining any lattice point in Λ as a point in Λ', offset by a coset representative $\mathbf{c}$ that labels the coset membership of λ. This can be expressed as

$$\Lambda = \Lambda' + [\Lambda/\Lambda'], \tag{3A2.8}$$

meaning that for any $\lambda \in \Lambda$

$$\lambda = \lambda' + \mathbf{c}. \tag{3A2.9}$$

where $\mathbf{c}$ is the coset representative for the coset of Λ' containing λ. For multistage partition chains, the corresponding view of the decomposition is

$$\Lambda = \Lambda'' + [\Lambda/\Lambda'] + [\Lambda'/\Lambda''] \tag{3A2.10}$$

Here a specific lattice point is addressable as $\lambda = \lambda'' + \mathbf{c} + \mathbf{d}$. This representation provides a compact "formula" for describing complicated lattices.

Communication Efficiency

Before continuing with the description of other lattices in higher dimensions, we should connect the lattice discussion with the signal design problem for the additive Gaussian noise channel. In AWGN signaling, we know that ML decoding is equivalent to decoding the received N-dimensional point in signal space to the nearest (in Euclidean sense) signal point, here a lattice point. (Already this raises the question of whether finding the nearest point is easy—more on this later.) The unit cell will, in general, be an N-dimensional polyhedron having τ planar faces, with these planes being perpendicular bisectors of lines connecting a lattice point to its nearest neighbors. Thus, the distance from a lattice point to these planes is $d_{\min}/2$. Within each such polyhedron, we can inscribe an N-dimensional sphere of radius $d_{\min}/2$, and these spheres will kiss a number of other spheres equivalent to the kissing number. If we recall that the figure of merit for a signal set is the minimum squared distance between constellation points, normalized by the average energy $d_{\min}^2/E_s$, it becomes apparent that an efficient signal design is a dense arrangement of unit-radius spheres in N-dimensional space, which is the classical sphere-packing problem [19]. Actually, it is not quite this simple in digital communications, for the error probability depends not only on $d_{\min}$, but also on the number of nearest neighbors, which in high-dimensionality space will be seen to be rather large.

The error performance can be upper-bounded by again treating the error region as a union of half-spaces:

$$P_e \leq \tau Q\left[\frac{d_{\min}}{(2N_0)^{1/2}}\right], \tag{3A2.11}$$

where τ is the number of faces of the unit cell, or Voronoi cell. On the other hand, the error probability is lower bounded by the probability that noise carries a transmitted

point to the wrong side of a *single plane*:

$$P_e > Q\left[\frac{d_{\min}}{(2N_0)^{1/2}}\right] \tag{3A2.12a}$$

Lower bounds differ only by a (perhaps large) multiplier. Nonetheless, the two bounds are exponentially equivalent, so *at high SNR* the signal design problem reverts to packing as many spheres as possible into a given N-dimensional volume.

We can clearly illustrate with a study of two-dimensional arrangements. Consider a large region of the plane bounded by a circle, enforcing a peak energy constraint on lattice points. By comparing the area of the unit cell for $\mathbf{Z}^2$ and $\mathbf{A}_2$, we find that the latter is about 15% smaller, while still maintaining the same $d_{min} = 1$. Thus, in a large circular region the hexagonal lattice is capable of placing 15% more points. (Essentially, hexagons are more circular than are squares.) Equivalently, if we fix the number of lattice points desired, the circular region can be 15% smaller in area in the case of $\mathbf{A}_2$, or about 7% smaller in radius. We have earlier seen that, for a given number of signal space points M, the figure of merit for detection efficiency is $d_{\min}^2/E_s$, where E_s is the peak (or average) energies expended by the signal set. Since peak and average energies are proportional to radius squared, and $\mathbf{A}_2$ has the same $d_{\min}$ as $\mathbf{Z}^2$, we conclude that the hexagonal lattice design is roughly 15%, or 0.7 dB, more energy efficient. Obviously, there are edge effects to deal with in finite constellation constructions that alter this slightly.

We now generalize this notion of communication efficiency for a lattice. Forney [52] defines the ***fundamental coding gain*** $\gamma(\Lambda)$ of a lattice as

$$\gamma(\Lambda) = \frac{d_{\min}^2(\Lambda)}{V(\Lambda)^{2/N}}. \tag{3A2.13}$$

$\gamma(\Lambda)$ is dimensionless and is easily shown to be invariant to scaling, rotation, and Cartesian product operations on lattices [52].

$\gamma(\Lambda)$ is the asymptotic coding gain obtained by adoption of constellations based on Λ *relative to the use of constellations from* $\mathbf{Z}^N$. To see why, consider constellations with M points in N dimensions, with M large. We choose the M points from the lattice as those points inside an N-dimensional sphere. (This minimizes peak and average energy values.) The volume of the sphere including M points from $\mathbf{Z}^N$ is about M, since the unit cell has volume 1. (We are allowed to neglect edge effects by requiring M to be large.) Similarly, the volume for a signal constellation based on Λ is $MV(\Lambda)$. The ratio of radii of the two spherical regions will then be

$$\frac{r_{\mathbf{Z}^N}}{r_\Lambda} = \frac{1}{V(\Lambda)^{1/N}}, \tag{3A2.14}$$

since the N-dimensional volume of a sphere varies as the Nth power of the radius. Since peak energy is proportional to radius-squared,[40]

$$\frac{E_{\mathbf{Z}^N}}{E_\Lambda} = \frac{1}{V(\Lambda)^{2/N}}. \tag{3A2.15}$$

[40]The same ratio holds for average energy if we treat the signal points as a uniform continuum in N-space.

The figure-of-merit for any constellation is $d^2_{\min}/E$, implying that the improvement afforded by constellations derived from Λ relative to those from $\mathbf{Z}^N$ is

$$\begin{aligned}\gamma(\Lambda) &= \frac{d^2_{\min}(\Lambda)/E_\Lambda}{d^2_{\min}(\mathbf{Z}^N)/E_{\mathbf{Z}^N}} \\ &= \frac{d^2_{\min}(\Lambda)}{V(\Lambda)^{2/N}}\end{aligned} \tag{3A2.16}$$

since $d_{\min}(\mathbf{Z}^N) = 1$. We caution that this is an argument based on large constellations.

Determination of the shape and thus the volume of the Voronoi cell can be somewhat tedious for high-dimensional lattices, but a lemma of Forney [52] is that, if Λ' is a sublattice of Λ of order p, then the volume of the Voronoi cell for Λ', whatever its shape, is

$$V(\Lambda') = pV(\Lambda) \tag{3A2.17}$$

This is a direct result of the partitioning of the total volume into Voronoi cells for the sublattice and its cosets. In particular, if Λ is a sublattice of order p of $\mathbf{Z}^N$, then $V(\Lambda) = p$. This immediately reveals that the volume of the Voronoi cell for $\mathbf{D}_4$ is 2, since the lattice is a partition of order 2 of $\mathbf{Z}^4$. It also tells us the volume of the dodecahedra surrounding points in $\mathbf{D}_3$ is 2, since $\mathbf{D}_3$ is a two-way partition of $\mathbf{Z}^3$.

We can now find the efficacy of the $\mathbf{D}_4$ lattice by recalling that $\mathbf{Z}^4/\mathbf{D}_4$ is a partition of order 2; that is, $\mathbf{Z}^4 = \mathbf{D}_4 \cup \mathbf{D}_4 + (1, 0, 0, 0)$. Thus, by the volume property given previously, $V(\mathbf{D}_4) = 2V(\mathbf{Z}^4) = 2$, and since $d^2_{\min} = 2$ as already determined, we have

$$\gamma(\mathbf{D}_4) = \frac{2}{2^{1/2}} = 2^{1/2}, \tag{3A2.18}$$

which in decibel units is about 1.5 dB. We should exercise some caution here, for the kissing number of $\mathbf{D}_4$ is 24, slightly larger than that of $\mathbf{Z}^4$. Still the asymptotic energy efficiency gain of (large) $\mathbf{D}_4$-based constellations is predicted to be 1.5 dB.

A concrete example of a design that exploits this potential is provided by a 256-point constellation selected from $\mathbf{D}_4$. This design would have the same spectral efficiency, or dimensionality per bit, as a 16-point QAM ($\mathbf{Z}^2$) construction. We begin by first translating the lattice by $(1, 0, 0, 0)$ and then retain the five lowest-energy orbital shells in the lattice. This can be shown to include exactly 256 points. The minimum squared distance between lattice points is still 2, and by calculation the average energy expended per symbol is 6.75 units. Using (3A2.11) and the fact that $E_s = 8E_b$, an upper bound on symbol error probability for this design would be

$$P_e \le 24Q\left[\left(1.19\frac{E_b}{N_0}\right)^{1/2}\right], \tag{3A2.19}$$

since the decision zone for each lattice point, excepting points on the periphery, is a 24-sided polyhedron. (The bound remains valid even with these edge effects.) Recalling the efficiency measure for 16-QAM derived in Section 3.3, we find the asymptotic energy efficiency relative to 16-QAM is 1.7 dB, slightly greater than the projected 1.5 dB. To

be fair, we should note that the multiplier coefficient for $\mathbf{Z}^2$ constellations is 4, and slightly better 16-point two-dimensional designs are available, especially if we switch to the $\mathbf{A}_2$ constellation.

Still Better Lattices

The lattice $\mathbf{E}_8$, known as the Gosset lattice, is a sublattice of $\mathbf{Z}^8$, known to be the densest eight-dimensional lattice packing, and is defined as follows. We first divide $\mathbf{Z}^8$ into $\mathbf{D}_8$ and a coset of $\mathbf{D}_8$. (As for all $\mathbf{D}_n$ lattices, $\mathbf{D}_8$ is the set of integer-valued 8-tuples whose coordinate sum is 0, mod 2.) Then $\mathbf{E}_8$ is the lattice defined as

$$\mathbf{E}_8 = 2\mathbf{D}_8 \cup 2\mathbf{D}_8 + (1, 1, 1, 1, 1, 1, 1, 1). \tag{3A2.20}$$

A partition chain involving $\mathbf{E}_8$ is $\mathbf{Z}^8/\mathbf{D}_8/2\mathbf{D}_8^*/\mathbf{E}_8/R\mathbf{D}_8/R\mathbf{D}_8^*/2\mathbf{Z}^8$, with $d_{\min}^2$ profile 1/2/2/4/4/4/4 [52]. (The lattice $\mathbf{D}_8^*$ is defined by

$$\mathbf{D}_8^* = \mathbf{D}_8 \cup \mathbf{D}_8 + \left(\frac{1}{2}, \frac{1}{2}, \frac{1}{2}, \frac{1}{2}, \frac{1}{2}, \frac{1}{2}, \frac{1}{2}, \frac{1}{2}\right) \cup \mathbf{D}_8$$
$$+ \left(\frac{1}{2}, \frac{1}{2}, \frac{1}{2}, \frac{1}{2}, \frac{1}{2}, \frac{1}{2}, \frac{1}{2}, -\frac{1}{2}\right) \cup \mathbf{D}_8 + (0, 0, 0, 0, 0, 0, 0, 1).$$

Therefore, $\mathbf{Z}^8/\mathbf{E}_8$ has order 16, from which it follows that $V(\mathbf{E}_8) = 16$. Also, the minimum squared distance between points in $\mathbf{E}_8$ is 4, as defined above, and this implies that the fundamental coding gain is

$$\gamma(\mathbf{E}_8) = \frac{4}{16^{2/8}} = 2, \tag{3A2.21}$$

or 3 dB, 1.5 dB better than the $\mathbf{D}_4$ lattice. The kissing number for $\mathbf{E}_8$ is 240. Table 3A2.1 lists a generator matrix for $\mathbf{E}_8$.

The reader should be suspicious by now that better things are possible in higher-dimensionality lattices and predict that doubling the dimension again might bring another 1.5 dB in fundamental coding gain. This prediction is correct, and the lattice is designated Λ_{16} and is a member of a sequence of Barnes–Wall lattices of dimension $N = 2^n$. Λ_{16} is a sublattice of $\mathbf{Z}^{16}$ of partition order 4096, with kissing number 4320, fundamental volume 4096, minimum squared distance of 8, and fundamental coding gain of $2^{3/2}$, or 4.5 dB. To achieve the same spectral efficiency as a design with 16 points in two-dimensions, the 16-dimensional constellation would require 2^{32} points from the lattice Λ_{16}, which clearly points to potential decoding issues.

The story goes on, and the next especially interesting case is the 24-dimensional Leech lattice, whose fundamental coding gain is 6.0 dB and upon which a modem has been developed [54].

In Table 3A2.1 we summarize the important parameters for the lattices discussed thus far, including $d_{\min}$, generator matrices, and the lattice density, the ratio of sphere volume to Voronoi cell volume, which curiously decreases with increasing dimension, even for best packings. In Figure 3A2.4, we summarize partition chains for the lattices described here. Some data are taken from [52] and [53].

TABLE 3A2.1 SUMMARY OF IMPORTANT LATTICES

N	Designation	Density, Δ	Kissing number	Fundamental Coding Gain, dB
1	$\mathbf{Z}$	1.0	2	0.0
2	$\mathbf{Z}^2 \sim \mathbf{D}_2$	0.785	4	0.0
2	$\mathbf{A}_2$ (hex)	0.907	6	0.5
3	$\mathbf{D}_3$ (fcc)	0.741	12	1.0
4	$\mathbf{D}_4$ (Schlafli)	0.617	24	1.5
8	$\mathbf{E}_8$ (Gosset)	0.254	240	3.0
16	Λ_{16} (B–W)	0.0147	4,320	4.5
24	Λ_{24} (Leech)	0.00193	196,560	6.0

$$\mathbf{A}_2\text{:}\quad \mathbf{M} = \begin{bmatrix} 1 & 0 \\ \frac{1}{2} & \frac{3^{1/2}}{2} \end{bmatrix}; \qquad \mathbf{D}_3\text{:}\quad \mathbf{M} = \begin{bmatrix} 2 & 0 & 0 \\ 1 & 0 & 1 \\ 0 & 1 & 1 \end{bmatrix};$$

$$\mathbf{D}_4\text{:}\quad \mathbf{M} = \begin{bmatrix} 2 & 0 & 0 & 0 \\ 1 & 0 & 0 & 1 \\ 0 & 1 & 0 & 1 \\ 0 & 0 & 1 & 1 \end{bmatrix}; \qquad \mathbf{E}_8\text{:}\quad \mathbf{M} = \begin{bmatrix} 2 & 0 & 0 & 0 & 0 & 0 & 0 & 0 \\ 0 & 2 & 0 & 0 & 0 & 0 & 0 & 0 \\ 0 & 0 & 2 & 0 & 0 & 0 & 0 & 0 \\ 0 & 0 & 0 & 2 & 0 & 0 & 0 & 0 \\ 1 & 0 & 0 & 0 & 1 & 1 & 0 & 1 \\ 0 & 1 & 0 & 0 & 1 & 0 & 1 & 1 \\ 0 & 0 & 1 & 0 & 0 & 1 & 1 & 1 \\ 0 & 0 & 0 & 1 & 1 & 1 & 1 & 0 \end{bmatrix}$$

$$\Lambda_{16}\text{:}\quad \mathbf{M}_{16} = \begin{bmatrix} 4 & 0 & 0 & 0 & 0 & 0 & 0 & 0 & 0 & 0 & 0 & 0 & 0 & 0 & 0 & 0 \\ 2 & 2 & 0 & 0 & 0 & 0 & 0 & 0 & 0 & 0 & 0 & 0 & 0 & 0 & 0 & 0 \\ 2 & 0 & 2 & 0 & 0 & 0 & 0 & 0 & 0 & 0 & 0 & 0 & 0 & 0 & 0 & 0 \\ 2 & 0 & 0 & 2 & 0 & 0 & 0 & 0 & 0 & 0 & 0 & 0 & 0 & 0 & 0 & 0 \\ 2 & 0 & 0 & 0 & 2 & 0 & 0 & 0 & 0 & 0 & 0 & 0 & 0 & 0 & 0 & 0 \\ 2 & 0 & 0 & 0 & 0 & 2 & 0 & 0 & 0 & 0 & 0 & 0 & 0 & 0 & 0 & 0 \\ 2 & 0 & 0 & 0 & 0 & 0 & 2 & 0 & 0 & 0 & 0 & 0 & 0 & 0 & 0 & 0 \\ 2 & 0 & 0 & 0 & 0 & 0 & 0 & 2 & 0 & 0 & 0 & 0 & 0 & 0 & 0 & 0 \\ 2 & 0 & 0 & 0 & 0 & 0 & 0 & 0 & 2 & 0 & 0 & 0 & 0 & 0 & 0 & 0 \\ 2 & 0 & 0 & 0 & 0 & 0 & 0 & 0 & 0 & 2 & 0 & 0 & 0 & 0 & 0 & 0 \\ 2 & 0 & 0 & 0 & 0 & 0 & 0 & 0 & 0 & 0 & 2 & 0 & 0 & 0 & 0 & 0 \\ 1 & 1 & 1 & 1 & 0 & 1 & 0 & 1 & 1 & 0 & 0 & 1 & 0 & 0 & 0 & 0 \\ 0 & 1 & 1 & 1 & 1 & 0 & 1 & 0 & 1 & 1 & 0 & 0 & 1 & 0 & 0 & 0 \\ 0 & 0 & 1 & 1 & 1 & 1 & 0 & 1 & 0 & 1 & 1 & 0 & 0 & 1 & 0 & 0 \\ 0 & 0 & 0 & 1 & 1 & 1 & 1 & 0 & 1 & 0 & 1 & 1 & 0 & 0 & 1 & 0 \\ 1 & 1 & 1 & 1 & 1 & 1 & 1 & 1 & 1 & 1 & 1 & 1 & 1 & 1 & 1 & 1 \end{bmatrix}$$

Density is defined as the ratio of sphere volume to Voronoi region volume.

Finding the Closest Lattice Point

For lattices to have utility as large constellations, efficient demodulation schemes must exist; specifically, given projection of the received signal into N-dimensional signal space, finding the closest lattice point must be relatively easy. After Sloane and Conway, we give algorithms for $\mathbf{D}_4$ and $\mathbf{E}_8$ and then generalize.

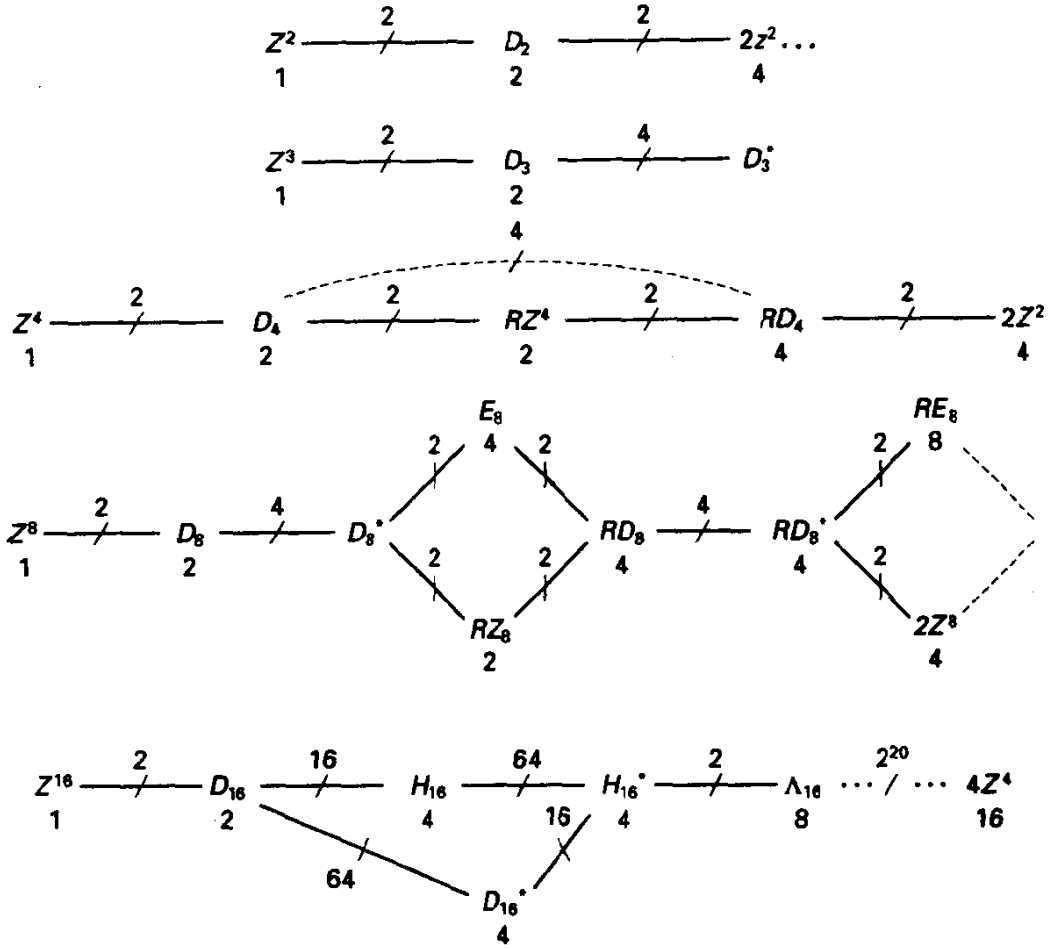

Figure 3A2.4 Partition chains for lattices. Number shown below lattice denotes d_{min}; number on branch denotes order of partition.

For $\mathbf{D}_4$, given $\mathbf{r}$, the nearest lattice point is found by first rounding each coordinate of $\mathbf{r}$ to an integer and checking whether the sum of the coordinates is 0, mod 2. If so, we have found the closest lattice point; if not, we round the position of the coordinate of $\mathbf{r}$ that rounded in the worst manner in the other direction. This will produce an integer vector meeting the constraints. Thus, "fast" decoding is no more complicated than two N-dimensional rounding operations.

Fast decoding in $\mathbf{E}_8$ proceeds as follows. We first find the nearest point in $2\mathbf{D}_8$, using a procedure similar to that described for $\mathbf{D}_4$. We also find the closest point in the translate $2\mathbf{D}_8 + (1, 1, 1, 1, 1, 1, 1, 1)$. The overall winner is obtained by computing the two Euclidean distances to the observed $\mathbf{r}$. Again, the structure of the lattice makes rapid decoding possible.

What really underlies these procedures is based on the coset decomposition. That is, if Λ can be decomposed into a sublattice and its cosets, finding the closest lattice point in Λ can be accomplished hierarchically: determine the closest point in each coset and then hold a run-off between the coset winners. Finding the closest point in a coset is

done as follows. Let $\Phi(\mathbf{r})$ be the function returning the closest point in a sublattice Λ'. Then the closest point to $\mathbf{r}$ in the coset $\Lambda' + \mathbf{c}$ is $\Phi(\mathbf{r} - \mathbf{c}) + \mathbf{c}$ [22]. Thus, if it is easy to find the closest point in the sublattices, and the number of such cosets is not too large, finding the nearest lattice point is relatively easy. Forney [52, part II] and others have also developed trellis-based algorithms that, particularly for large-dimensional lattices, can be more efficient than a coset description might suggest.

Reprise

Our view here is that lattices are merely a convenient means of implementing multidimensional signal constellations of M points. We might alternatively view a lattice design as a coding technique with aspects of redundancy and memory, however. DeBuda [56] has shown that lattice codes (with high dimensionality) can approach the channel capacity bound for the band-limited Gaussian channel. We might view the lattice signal design as a restricted selection of points from a modulator capable of synthesizing $\mathbf{Z}^N$, usually through $N/2$ consecutive uses of a $\mathbf{Z}^2$ constellation. Signal waveforms are selected by grouping a sequence of message bits and choosing a point from the sequence of modulator symbols. Thus, the construction exhibits the traditional attributes of block codes—redundancy and memory. This connection to block codes will be more striking later in the text, where we see these lattice codes, or signal designs, as obtained by having a short block coder operating on some of the message bits form a coset label, with the remaining bits used to select a member of the specified coset.

APPENDIX 3A3: DERIVATION OF POWER SPECTRUM

In this appendix we formulate a general expression for the power spectrum of the signal produced by a digital modulator. The earliest general formulation along these lines was apparently provided by Tausworthe and Welch [36], although a special case result was given earlier by Bennett [37].

Our treatment again represents the modulator output as a random process formed by the time superposition of modulator signals, as induced by the input sequence $\{x_n\}$.

$$s(t) = \sum_n s_{x_n}(t - nT_s). \tag{3A3.1}$$

The methodology can handle baseband or bandpass signals directly. There is, however, a subtle issue in the carrier modulation case relating to whether the carrier is synchronous in frequency with the symbol rate[41] so that the signal can indeed be represented as in (3A3.1). Usually, this synchronism does not exist, and in this case we shall find the power spectrum by analyzing the power spectrum of the baseband equivalent complex envelope signal and then translating to the carrier frequency according to the Fourier translation property. We will say more about this at the end.

[41] If synchronism is absent, the actual signal trajectories that the modulator may select differ from interval to interval.

We shall analyze a case wherein the inputs to the modulator obey a Markov model (Section 2.5), as would pertain for some forms of coding prior to modulation, either for error control or spectrum shaping. As an important special case, we have the independent input symbol model.

We assume there are M signals available at each symbol time, and if the modulator emits signal $s_i(t)$, we say the modulator input is in state i. The Markov structure on the input is governed by transition probabilities a_{ij}, denoting the conditional probability that the input symbol is j, given that the previous symbol is i. The steady-state probability vector $\mathbf{P} = (P_0, P_1, \ldots, P_{M-1})$ for a regular Markov chain is the solution to (2.5.43): $\mathbf{P} = \mathbf{PA}$. We let $P_i, i = 0, 1, \ldots, M-1$ denote the marginal probability that symbol i is input to the modulator.

To determine the power spectrum, we follow the route of determining the autocorrelation function and then Fourier transforming. The signal in (3A3.1) is, however, not wide sense stationary, lacking a randomization of the timing epoch. Such a signal is *cyclostationary*, meaning that the mean and autocorrelation function are periodic functions in t with period T_s. The mean and autocorrelation function for a "stationarized" version of this process are obtained by averaging over T_s seconds [57].

We begin with the definition of the autocorrelation function for complex signals:

$$\begin{aligned} R_s(t, t+\tau) &= E\left[s(t)s^*(t+\tau)\right] \\ &= E\left[\sum_n s_{X_n}(t - nT_s)\sum_m s^*_{X_m}(t - mT_s + \tau)\right] \qquad \text{(3A3.2a)} \\ &= \sum_{i=0}^{M-1}\sum_{j=0}^{M-1}\sum_n\sum_m P[X_n = i, X_m = j]s_i(t - nT_s)s_j^*(t - mT_s + \tau). \end{aligned}$$

By the Markov property the required joint probability is $P[X_n = i, X_m = j] = P_i a_{ij}^{(m-n)}$, where $a_{ij}^{(m-n)}$ is the (i, j)th entry in the multistep transition matrix $\mathbf{A}^{m-n}$. Therefore,

$$R_s(t, t+\tau) = \sum_i\sum_j\sum_n\sum_m P_i a_{ij}^{(m-n)} s_i(t - nT_s)s_j^*(t - mT_s + \tau). \qquad \text{(3A3.2b)}$$

The function $R_s(t, t+\tau)$ will be periodic in t with period T_s for any fixed τ. To obtain the standard autocorrelation function, we integrate over one period:

$$\begin{aligned} R_s(\tau) &= \frac{1}{T_s}\int_0^{T_s} R_s(t, t+\tau)\,dt \\ &= \frac{1}{T_s}\sum_i\sum_j\sum_n\sum_m P_i a_{ij}^{(m-n)}\int_0^{T_s} s_i(t - nT_s)s_j^*(t - mT_s + \tau)\,dt \\ &= \frac{1}{T_s}\sum_i\sum_j\sum_n\sum_m P_i a_{ij}^{(m-n)}\int_{-nT_s}^{(1-n)T_s} s_i(u)s_j^*[u + (n-m)T_s + \tau]\,du. \end{aligned} \qquad \text{(3A3.3)}$$

We rewrite (3A3.3) as

$$R_s(\tau) = \frac{1}{T_s}\sum_i\sum_j P_i\sum_n\int_{-nT_s}^{(1-n)T_s} s_i(u)\left[\sum_m a_{ij}^{(m-n)}s_j^*(u - (m-n)T_s + \tau)\right]dt \qquad \text{(3A3.4)}$$

This can be finally reduced to

$$R_s(\tau) = \frac{1}{T_s} \sum_i \sum_j \int_{-\infty}^{\infty} P_i s_i(u) \left[\sum_{k=-\infty}^{\infty} a_{ij}^{(k)} s_j^*(u - kT_s + \tau) \right] du, \tag{3A3.5}$$

which is one expression of the desired autocorrelation function. Observe that knowledge of the signal set and the Markov structure of the input allows numerical computation of the autocorrelation function.

The autocorrelation function derived here will have an aperiodic component, $R^{\text{aper}}(\tau)$, decaying to zero as $\tau \to \infty$, and may have a periodic, or persistent, component, $R_s^{\text{per}}(\tau)$. These will produce continuum and discrete, or spectral line, contributions to the power spectrum, respectively. The periodic portion may be found by observing the limiting behavior of $R_s(\tau)$ as τ becomes large. It is known that this can be determined from the product of the process means at time t and $t+\tau$. When averaged over a period, we get

$$R_s^{\text{per}}(\tau) = \frac{1}{T_s} \int_0^{T_s} E[s(t)] E[s^*(t+\tau)]\, dt. \tag{3A3.6}$$

Now the mean function $E[s(t)]$ is also periodic with period T_s and may therefore be expressed with a Fourier series:

$$E[s(t)] = \sum_{k=-\infty}^{\infty} C_k e^{j2\pi kt/T_s}, \tag{3A3.7}$$

where the Fourier coefficients are

$$\begin{aligned} C_k &= \frac{1}{T_s} \int_0^{T_s} E[s(t)]\, e^{-j2\pi kt/T_s}\, dt = \frac{1}{T_s} \left[\sum_{i=0}^{M-1} P_i s_i(t) \right] e^{-j2\pi kt/T_s}\, dt \\ &= \frac{1}{T_s} \sum_{i=0}^{M-1} P_i S_i\left(\frac{k}{T_s}\right) \end{aligned} \tag{3A3.8}$$

and where $S_i(f)$ is the Fourier transform of $s_i(t)$. Substituting this into (3A3.6) yields the periodic portion of the autocorrelation function:

$$\begin{aligned} R_s^{\text{per}}(\tau) &= \frac{1}{T_s} \int_0^{T_s} \sum_k C_k e^{j2\pi kt/T_s} \sum_l C_l^* e^{-j2\pi l(t+\tau)/T_s}\, dt \\ &= \frac{1}{T_s} \sum_{m=-\infty}^{\infty} |C_m|^2 e^{-j2\pi m\tau/T_s}, \end{aligned} \tag{3A3.9}$$

where we have employed orthogonality of the complex exponentials. This function will have a Fourier transform comprised solely of spectral lines:

$$G_{s_d}(f) = \frac{1}{T_s^2} \sum_{m=-\infty}^{\infty} \left| \sum_{i=0}^{M-1} P_i S_i\left(\frac{m}{T_s}\right) \right|^2 \delta\left(f - \frac{m}{T_s}\right). \tag{3A3.10}$$

Notice that spectral lines may appear only at multiples of the symbol rate.

The aperiodic portion of the correlation function is the remainder of (3A3.5) after removal of the periodic part, and upon taking the Fourier transform of this remainder,

we find that the *continuum* portion of the spectrum is

$$G_{s_c}(f) = \frac{1}{T_s} \sum_{i=0}^{M-1} \sum_{j=0}^{M-1} P_i S_i(f) S_j^*(f) \left\{ \sum_{m=-\infty}^{\infty} (a_{ij}^{(m)} - P_j) e^{-j2\pi f m T_s} \right\}. \tag{3A3.11}$$

Putting together the discrete and continuum components, we obtain the complete expression

$$\begin{aligned} G_s(f) = {} & \frac{1}{T_s} \sum_i \sum_j P_i S_i(f) S_j^*(f) \left[\sum_{m=-\infty}^{\infty} (a_{ij}^{(m)} - P_j) e^{-j2\pi f m T_s} \right] \\ & + \frac{1}{T_s^2} \sum_{m=-\infty}^{\infty} \left| \sum_{i=0}^{M-1} P_i S_i\left(\frac{m}{T_s}\right) \right|^2 \delta\left(f - \left(\frac{m}{T_s}\right)\right). \end{aligned} \tag{3A3.12}$$

Notice that this expression is completely determined by the signal set and the Markov chain transition probabilities. In evaluating this expression, we need to interpret $\mathbf{A}^0 = \mathbf{I}$.

There are several important cases of this result. First, suppose that all signals are scalar multiples, denoted A_i, of some common pulse shape $\phi_0(t)$, as in M-PAM of M-QAM. Then (3A3.12) reduces to

$$\begin{aligned} G_s(f) = {} & \frac{1}{T_s} |\Phi_0(f)|^2 \sum_i \sum_j P_i A_i A_j^* \sum_{m=-\infty}^{\infty} (a_{ij}^{(m)} - P_j) e^{-j2\pi f m T_s} \\ & + \frac{1}{T_s^2} |\Phi_0(f)|^2 \left| \sum_i P_i A_i \right|^2 \sum_{m=-\infty}^{\infty} \delta\left(f - \frac{m}{T_s}\right). \end{aligned} \tag{3A3.13}$$

Bennett [37] first derived this expression in different form.

Another important case is that for which the input symbols are assumed *independent*, but signals have arbitrary shape. Independence in the model implies

$$a_{ij}^{(m)} = \begin{cases} P_j, & m \neq 0, \\ 1, & m = 0. \end{cases}$$

Simplification then gives

$$\begin{aligned} G_s(f) = {} & \frac{1}{T_s} \left[\sum_i P_i |S_i(f)|^2 - \left| \sum_i P_i S_i(f) \right|^2 \right] \\ & + \frac{1}{T_s^2} \sum_{m=-\infty}^{\infty} \left| \sum_i P_i S_i(f) \right|^2 \delta\left(f - \frac{m}{T_s}\right). \end{aligned} \tag{3A3.14}$$

Invoking both these assumptions gives

$$\begin{aligned} G_s(f) = {} & \frac{1}{T_s} |\Phi_0(f)|^2 \left(\sum_i P_i |A_i|^2 - \left| \sum_i P_i A_i \right|^2 \right) \\ & + \frac{1}{T_s^2} |\Phi_0(f)|^2 \left| \sum_i P_i A_i \right|^2 \sum_{m=-\infty}^{\infty} \delta\left(f - \frac{m}{T_s}\right). \end{aligned} \tag{3A3.15}$$

In all cases it is interesting to note that the spectral line contribution depends only on the signal Fourier transforms and the marginal probabilities, but not the transition probabilities directly.

As an application, and one that highlights the synchronism issue mentioned earlier, consider binary on–off keying of a sinusoidal carrier. Let the pulse shape be rectangular with bit duration T_b. Suppose that the carrier frequency is exactly an integral multiple k of the bit rate. Then the model of (3A3.1) pertains where

$$s_0(t) \equiv 0 \quad \text{and} \quad s_1(t) = A\cos\left(\frac{2\pi kt}{T_b}\right), \qquad 0 < t \le T_b. \tag{3A3.16}$$

If we assume that the input bits are equiprobable and independent, we may use (3A3.13) to obtain the power spectrum:

$$G_s(f) = \frac{A^2T_b}{16}\left[\frac{\sin^2\left[\pi\left(f-\frac{k}{T_b}\right)T_b\right]}{\left[\pi(f-\frac{k}{T_b})T_b\right]^2} + 2\frac{\sin\left[\pi(f-\frac{k}{T_b})T_b\right]\sin\left[\pi(f+\frac{k}{T_b})\right]}{\pi^2\left(f-\frac{k}{T_b}\right)\left(f+\frac{k}{T_b}\right)T_b^2}\right.$$
$$\left. + \frac{\sin^2\left[\pi\left(f+\frac{k}{T_b}\right)T_b\right]}{\left[\pi\left(f+\frac{k}{T_b}\right)T_b\right]^2}\right] + \frac{A^2}{16}\left[\delta\left(f-\frac{k}{T_b}\right)+\delta\left(f+\frac{k}{T_b}\right)\right]. \tag{3A3.17}$$

Suppose, on the other hand, that there is lack of synchronism between carrier frequency and bit rate; then in any given bit interval the amount of phase change experienced by the carrier phase is not an integral multiple of 2π radians, and the superposition model of (3A3.1) is not strictly valid because signals at later times are not mere translates of the signal available at, say, time 0. To handle this case, we write the modulator output as

$$s(t) = \mathrm{Re}\left\{\tilde{s}(t)e^{j(2\pi f_c t+\Theta)}\right\}, \tag{3A3.18}$$

where $\tilde{s}(t)$ is the complex envelope signal

$$\tilde{s}(t) = \begin{cases} 0, & x_n = 0 \\ A, & x_n = 1 \end{cases}, \qquad nT_b < t < (n+1)T_b, \tag{3A3.19}$$

and Θ is a uniformly distributed phase angle. The power spectrum of the complex envelope signal is that of a real unipolar NRZ signal and has a spectral line at zero frequency plus a continuum component:

$$G_{\tilde{s}}(f) = \frac{A^2}{4}\delta(f) + \frac{A^2T_b}{4}\frac{\sin^2(\pi fT_b)}{(\pi fT_b)^2}. \tag{3A3.20}$$

The power spectrum for $s(t)$ in this case is then given by

$$G_s(f) = \frac{1}{4}\left[G_{\tilde{s}}(f-f_c) + G_{\tilde{s}}^*(-f-f_c)\right], \tag{3A3.21}$$

which is just two translated copies of the baseband power spectrum. The power spectrum of (3A3.21) is slightly different than that obtained in (3A3.17), although the differences diminish when $k \gg 1$. Both results give the same total power, however. In both cases the rate of decay of the power spectrum for large separations from f_c is of the form f^{-2}, resulting from signal discontinuity.

A seemingly innocuous change to the original formulation, $s_1(t) = A\sin(2\pi kt/T_b)$, makes the signal continuous everywhere and changes the asymptotic spectral rate of decay to f^{-4}. Lack of carrier synchronism alters this, however, back to the preceding situation, due to possible discontinuity. Clearly, many subtleties are involved.

BIBLIOGRAPHY

1. Haykin, S., *Communication Systems*, 2nd ed., New York: Wiley, 1983.
2. Brayer, K., *Fading Communication Channels*, New York: IEEE Press. See also *IEEE Journal of Selected Areas in Communication*, February, 1987, issue devoted to communication on fading channels.
3. Jakes, W. C., Jr., *Microwave Mobile Communications*, New York: Wiley, 1974.
4. Van der Ziel, A., *Noise*, Englewood Cliffs, NJ: Prentice Hall, 1986.
5. Rummler, W. D., Coutts, R. P., amd Liniger, M., "Multipath Fading Channel Models for Microwave Digital Radio," *IEEE Communications Magazine*, vol. 24, no. 11, pp. 30–42, 1986. See also *IEEE Journal of Selected Areas in Communication*, April 1987, issue devoted to digital radio.
6. Wozencraft, J. M., and Jacobs, I. M., *Principles of Communication Engineering*, New York: Wiley, 1965.
7. Franks, L. E., *Signal Theory*, Englewood Cliffs, NJ: Prentice Hall, 1969.
8. Weber, C. L., *Elements of Detection and Signal Design*, New York: Springer-Verlag, 1987.
9. The Gram–Schmidt procedure is found in many applied mathematics texts; Reference 6 contains an excellent appendix 4A.
10. Loeve, M., *Probability Theory*, New York: Van Nostrand, Reinhold, 1955. (Also found in [1].)
11. Viterbi, A. J., "On Coded Phase Coherent Communication," *IRE Trans. Space Electronics Telemetry*, vol. SET-7, pp. 3–12, March 1961.
12. Lindsey, W. C., and Simon, M. K., *Telecommunications Systems Engineering*, Englewood Cliffs, NJ: Prentice Hall, 1972.
13. Hughes, L. W., "Tighter Bound on Error Probability for Orthogonal Signals," *IEEE Trans. Information Theory*, vol. 40, no. 4, p. 670, April 1992.
14. Arthurs, E., and Dym, H., "On the Optimum Detection of Digital Signals in the Presence of White Gaussian Noise—A Geometric Interpretation and a Study of Three Basic Data Transmission Systems," *IRE Trans. Communication Systems*, vol. CS-10, no. 4, pp. 336–372, Dec. 1962.
15. Wu, W., *Digital Satellite Communications*, Rockville, MD: Computer Science Press, 1984.
16. Forney, G. D., Jr., Gallager, R. G., Lang, G. R., Longstaff, F. M., and Qureshi, S. U., "Efficient Modulation for Band-limited Channels," *IEEE Journal of Selected Areas in Communications*, vol. SAC-2, no. 5, pp. 632–647, September 1984.
17. Nogiuchi, T., Daido, Y., and Nossek, J. A., "Modulation Techniques for Microwave Digital Radio," *IEEE Communications Magazine*, vol. 24, no. 10, pp. 21–30, October 1986.
18. Steiner, M., "New Results in Signal Design for the AWGN Channel," *IEEE Intl. Symposium on Information Theory*, San Antonio, TX, 1993.
19. Sloane, N. J., "The Packing of Spheres," *Scientific American*, pp. 116–125, January 1984.

20. Foschini, G. J., Gitlin, R. D., and Weinstein, S. B., "Optimization of Two-dimensional Signal Constellations in the Presence of Gaussian Noise," *IEEE Trans. Communications*, vol. COM-22, pp. 28–38, 1974.
21. Simon, M. K., and Smith, J. G., "Hexagonal Multiple Phase and Amplitude Shift-keyed Signal Sets," *IEEE Trans. Communications*, vol. COM-21, pp. 1108–1115, October 1973.
22. Conway, J. H., and Sloane, N. J. A., "Fast Quantizing and Decoding for Lattice Quantizers and Codes," *IEEE Trans. Information Theory*, vol. IT-28, pp. 227–232, 1982.
23. Wilson, S. G., Sleeper, H. A., and Srinath, N. K., "Four-dimensional Modulation and Coding: An Alternate to Frequency Reuse," *IEEE Intl. Conference Communication Record*, Amsterdam, 1984.
24. Lucky, R. W., Salz, J., and Weldon, E. J., *Principles of Data Communication*, 1968.
25. Abramowitz, M., and Stegun, I., *Handbook of Mathematical Functions*, New York: Dover, 1970.
26. Viterbi, A. J., *Principles of Coherent Communications*, New York: McGraw-Hill, 1966.
27. Van Trees, H. L., *Detection, Estimation and Modulation Theory, Part I*, New York: Wiley, 1968.
28. Salz, J., and Saltzberg, B., "Double Error Rates in Differentially Coherent Phase Systems," *IRE Trans. Communication Systems*, vol. CS-12, pp. 202–205, June 1964.
29. Oberst, J. F., and Schilling, D. L., "Double Error Probability in Differential PSK," *Proc. IEEE*, pp. 1099–1100, June 1968.
30. Pawula, R. F., Rice, S. O., and Roberts J. H., "Distribution of the Phase Angle between Two Vectors Perturbed by Gaussian Noise," *IEEE Trans. Communications*, vol. COM-30, no. 8, pp. 1828–1841, 1982.
31. Proakis, J., *Digital Communications*, 2nd Ed., New York: McGraw-Hill, 1988.
32. Henry, J. C., "DPSK Under Frequency Offset," *IEEE Trans. Communications*, 1972.
33. Divsalar, D., and Simon, M. K., "Multiple Symbol Differential Detection of MPSK," *IEEE Trans. Communications*.
34. Wilson, S. G., Freebersyser, J., and Marshall, C., "Multi-symbol Detection of M-DPSK," *IEEE Globecom Conference Record*, Dallas, TX, 1989.
35. Amoroso, F., "The Bandwidth of Digital Data Signals," *IEEE Communications Magazine*, vol. 18, pp. 13–24, November 1980.
36. Tausworthe, R., and Welch, L. R., "Power Spectra of Signals Modulated by Random and Pseudorandom Sequences," Jet Propulsion Laboratory Technical Report 32–140, Pasadena, CA, 1961.
37. Bennett, W. R., "Statistics of Regenerative Digital Transmission," *Bell System Tech. J.*, pp. 1585–1594, November 1958.
38. Nyquist, H., "Certain Topics in Telegraph Transmission Theory," *AIEE Trans.* vol. 47, pp. 617–644, 1928.
39. Papoulis, A., *The Fourier Integral and Its Applications*, New York: McGraw-Hill, 1962.
40. Landau, H. J., and Pollak, H., "Prolate Spheroid Wave Functions, Fourier Analysis, and Uncertainty, Parts I, II, III," *Bell System Tech. Journal*, 1961–62.
41. Dixon, R. C., *Spread Spectrum Techniques*, New York: IEEE Press, 1976.
42. Simon, M. K., Omura, J. K., Scholz, R. A., and Levitt, B. K., *Spread Spectrum Communications*, Vols. I, II, and III, Computer Science Press, 1985.
43. Holmes, J. K., *Coherent Spread Spectrum Systems*, New York: Wiley-Interscience, 1982.

44. Golomb, S., *Shift Register Sequences*, San Francisco: Holden Day, 1967.

45. MacWilliams, F. J., and Sloane, N. J. A., "Pseudo-random Sequences and Arrays," *Proc. of IEEE*, vol. 64, pp. 1715–1729, December 1976.

46. Gold, R., "Optimal Binary Sequences for Spread Spectrum Multiplexing," *IEEE Trans. Information Theory*, vol. IT-13, pp. 619–621, October 1967.

47. Botzas, S., Hammons, S., and Kumar, P. V., "4-Phase Sequences with Near-Optimum Correlation Properties," *IEEE Trans. Information Theory*, vol. 38, pp. 1101–1113, May 1992.

48. Welch, L. R., "Lower Bounds on the Maximum Cross Correlation of Signals," *IEEE Trans. Information Theory*, vol. IT-20, pp. 397–399, May 1974.

49. Lehnert, J., and Pursky, M. B., "Error Probabilities for Binary Direct-Sequence Spread Spectrum Communication with Random Signature Sequences," *IEEE Trans. on Communications*, vol. 35, pp. 87–98. January 1987.

50. Geraniotis, E., and Ghaffari, B., "Performance of Binary and Quaternary Direct-Sequence Spread Spectrum Multiple-Access Systems with Random Signature Sequences," *IEEE Trans. on Communications*, vol. 39, pp. 713–724, May 1991.

51. Viterbi, A. J., and Omura, J. K., *Principles of Digital Communications and Coding*, New York: McGraw-Hill, 1979.

52. Forney, G. D., Jr., "Coset Codes–Part I," *IEEE Trans. Information Theory*, vol. IT-34, 1988.

53. Conway, J. H., and Sloane, N. J. A., *Lattices, Sphere Packings, and Groups*, New York: Springer-Verlag, 1988.

54. Lang, G. R., and Longstaff, F. M., "A Leech Lattice Modem," *IEEE Journal of Selected Areas in Communications*, vol. 7, no. 6, pp. 968–973, August 1989.

55. deBuda, R., "Coding Theorem for Lattice Codes," *IEEE Trans. Information Theory*.

56. Bic, J. C., Duponteil, D., and Imbeaux, J. C., *Elements of Digital Communication*, New York: Wiley, 1991.

57. Gardner, W. A., and Franks, L. E., "Characterization of Cyclostationary Random Processes," *IEEE Trans. Information Theory*, vol. IT-21, pp. 4–15, January 1975.

58. Viterbi, A. J., "Spread Spectrum Communication—Myths and Realities," *IEEE Communications Magazine*, vol. 17, pp. 11–18, May 1979. (See also Viterbi, A. J., *IEEE Communications Magazine*, April 1985, for a sequel.)

59. Goldberg, B. (ed.), *Communication Channels: Characterization and Behavior*, New York: IEEE Press, 1976.

EXERCISES

3.1.1. Assume a channel can be described as having constant gain and linear phase over a range of frequencies, $[0, B]$ hertz; that is,

$$H(f) = Ge^{-j2\pi f\alpha}, \qquad |f| \leq B.$$

Using transform calculus, show this implies that the response to any input signal $s(t)$ having Fourier transform band-limited to B hertz will be $Gs(t - \alpha)$, which we define to be an undistorted replica of the input.

3.1.2. The Rayleigh fading model presumes that the instantaneous amplitude measured at the channel output is Rayleigh distributed. The square of the random quantity would be instantaneous

normalized power. In Chapter 2, we found that the square of a Rayleigh random variable had the one-sided exponential density function. The p.d.f. for $P(t) = A^2(t)$ at any time t is

$$f_P(p) = \frac{1}{P} e^{-p/P}, \qquad p \geq 0,$$

where P is the average power.

(a) Find the probability that the received power is less than a level 3 dB below the average power level P.

(b) Determine the probability that the power is less than a level 10 dB below the average level.

(c) Determine the probability that the power is more than 3 dB above the average power level.

3.1.3. Fading signals are often characterized by their *Doppler bandwidth* in the spectral domain and *decorrelation time* in the time domain. These channel descriptors are, respectively, the essential extent in frequency (or time) for which the power spectrum and correlation function of the complex fading process $A(t)e^{j\phi(t)}$ are essentially nonzero, and these descriptors are approximately reciprocally related.

(a) A mobile radio channel operating at 900-MHz center frequency with vehicle speeds of 100 km/h may exhibit Doppler bandwidths of 100 Hz. Find the decorrelation time, and determine if the fading is "slow" when the bit rate is 9600 bps.

(b) Repeat for a high-frequency (3 to 30 MHz) ionospheric channel, whose Doppler bandwidths are ordinarily less than 1 Hz. Here the fading process is due to turbulence in the ionospheric reflecting medium.

3.1.4. A typical radio channel may have a net loss between transmitter output and receiver input of 143 dB. If the transmitter output power is 5 W, determine the received power level. The noise power density $N_0/2$ is often characterized by an equivalent noise temperature, T_{sys}; that is,

$$\frac{N_0}{2} = \frac{kT_{\text{sys}}}{2},$$

where $k = 1.38 \cdot 10^{-23}$ is Boltzmann's constant. If $T_{\text{sys}} = 200$ K at this same point in the system, and the bit rate is $R = 1$ MHz, determine E_b/N_0 at the receiver.

3.2.1. Show that the squared L_2 distance, $d_{i,j}^2$, between waveforms $s_i(t)$ and $s_j(t)$; that is,

$$d_{i,j}^2 = \int_{T_i}^{T_f} \left[s_i(t) - s_j(t)\right]^2 dt,$$

is equal to the signal space distance between $\mathbf{s}_i$ and $\mathbf{s}_j$; that is,

$$d_{i,j}^2 = \sum_{m=0}^{N-1} \left[s_{im} - s_{jm}\right]^2.$$

Hint: Substitute $s_i(t) = \sum s_{im}\phi_m(t)$ in the integral expression for squared distance and simplify, employing orthogonality of the basis functions.

3.2.2. Show that the basis functions given in (3.2.11a), the phase-quadrature pair, are exactly orthonormal if ω_c is a multiple of $2\pi/T_s$. In practice, this is not usually the case; show, however, that if ω_c is very large relative to $2\pi/T_s$ then essential orthonormality is obtained.

3.2.3. A signal constellation with $M = 4$ points in two dimensions is shown in Figure P3.2.3a.

(a) Consider three choices of basis functions:

Case I: phase-quadrature sinusoids

Case II: two nonoverlapping pulses

Case III: the functions shown in Figure P3.2.3b

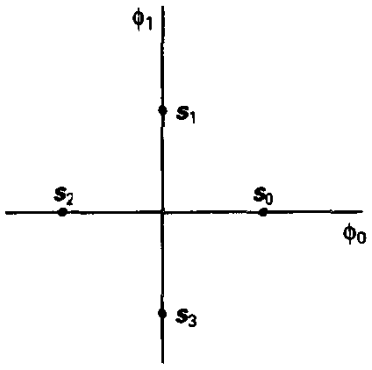

Figure P3.2.3a

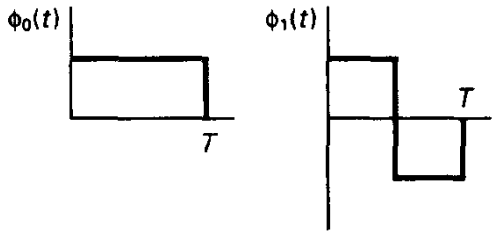

Figure P3.2.3b

Write expressions for or sketch the four signal waveforms in each case.

(b) Formulate upper and lower bounds on the symbol error probability for the AWGN channel as a function of E_b/N_0. Note that this depends only on the constellation and not the exact nature of the signal set employed.

(c) Evaluate both of these bounds when $E_b/N_0 = 10$ dB.

3.2.4. Use the Gram–Schmidt procedure to obtain a basis set for the signal pair of Figure P3.2.4. Find the signal-space coordinates of each signal, and verify that the intrasignal distance is the same in the L_2 sense as it is in signal space. Also verify that the signal energy is the square of the distance from the origin in signal space.

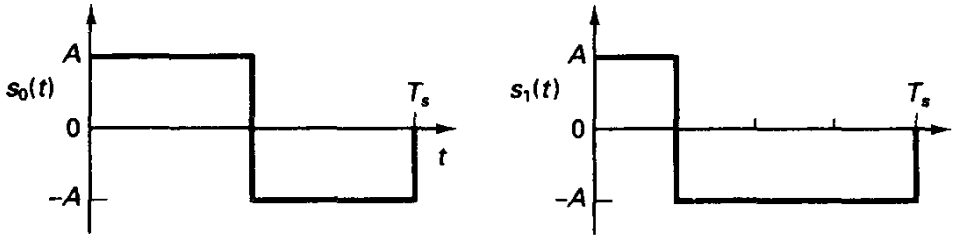

Figure P3.2.4

3.2.5. The following two signal sets have $M = 16$ points each: the MPSK set with

$$s_i(t) = A\cos\left(\omega_c t + \frac{2\pi i}{M}\right), \qquad i = 0, 1, \ldots, 15,$$

and the set with $s_i(t)$ specified by rows of the 16×16 Hadamard matrix, H_{16}. Sketch or describe the signal constellation for each, and determine the dimensionality of the signal set in units of dimensions per bit transmitted.

3.2.6. In binary frequency shift keying, suppose the two signals are represented as

$$s_0(t) = A\cos(\omega_c t + \Delta\omega t + \theta), \qquad 0 \le t \le T_s,$$

and $$s_1(t) = A\cos(\omega_c t - \Delta\omega t + \theta),$$

where $\Delta f = \Delta\omega/2\pi$ is the carrier frequency deviation in hertz. θ is a common phase angle that is known to the demodulator.

(a) Choose the first signal, normalized, as the first basis function, and locate the other signal in signal space as a function of Δf. (Assume that the carrier frequency is "large.") What deviation provides the largest distance? Note that it does not correspond to a situation where the signals are orthogonal; slight negative correlation is better.

(b) Show that $\Delta f = n/4T_s$ yields orthogonal signals. (Note that this condition holds only if both signals have the same starting phase; if the phases are different, as they would be in selecting from two different oscillators, the orthogonality condition is $\Delta f = n/2T_s$.)

3.3.1. Suppose a set of M low-pass signals is strictly band-limited to W hertz. One is sent and received in the presence of white Gaussian noise. Show that prefiltering the received signal $r(t)$ to a bandwidth of W hertz with an *ideal* LFF does not compromise the detection process. Equivalently, show that the noise signal outside this bandwidth is irrelevant. (*Hint*: The received signal could be viewed as being low pass filtered and high pass filtered, decomposing $r(t)$ into two component processes; does the high-pass filter output contain a signal-dependent portion, or is the noise correlated with the LPF output noise?)

3.3.2. Show that

$$\int_{T_i}^{T_f} r^{(N)}(t)s_i(t)\,dt = \sum_{m=0}^{N-1} r_m s_{im},$$

where r_m and s_{im} are coefficients of the N-term expansion for the received waveform and an N-dimensional signal, respectively. Argue that by padding the coefficients beyond s_{N-1} with zeros we can equivalently state that

$$\int_{T_i}^{T_f} r(t)s_i(t)\,dt = \sum_{m=0}^{N-1} r_m s_{im}.$$

3.3.3. If a signal set constrained in time to $[0, T_s]$ is to be detected in the presence of AWGN, the optimal receiver does not benefit by using the received signal $r(t)$ either prior to or after the signal. Why? Would the same be true if the noise was colored, that is, had a spectrum that was not constant for all frequencies? (*Hint*: The answers involve the principle of irrelevance.)

3.3.4. Consider the binary communication system shown in Figure P3.3.4, wherein during each bit interval T_s either a binary code waveform $c(t)$ or its logical complement phase-shift-keys the carrier. (This is commonly known as direct sequence spread-spectrum signaling.) Argue that the receiver must perform an antipodal decision, and sketch an implementation of the optimal receiver. You may invoke a genie to inform the receiver of the code sequence $c(t)$ and its "phase."

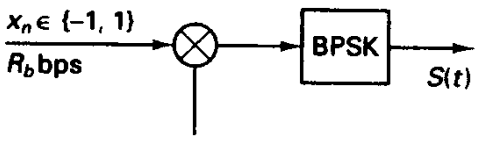

$c(t)$, a ± 1 code pattern with chip rate $R_c = mR_b$

Figure P3.3.4

3.3.5. In any on–off keying situation, if the receiver knows the received signal amplitude, the proper threshold may be set, and $P(\epsilon) = Q[(E_b/2N_0)^{\frac{1}{2}}]$, as discussed. If, however, the signal level is estimated incorrectly, suboptimal performance results. Examine the case where the receiver believes the signal level is half (in energy) the actual value, when the actual E_b/N_0 is 10 dB. Here one type of error event dominates the other.

3.3.6. In one-shot reception of a rectangular pulse in AWGN the optimal detector is an integrate-and-dump detector. This detector can be viewed as a low-pass filter, with normalized magnitude of the transfer function given by

$$|H_{\text{opt}}(f)| = \frac{|\sin(\pi f T_s)|}{(\pi f T_s)}.$$

Consider instead the use of a more familiar first-order low-pass filter whose transfer function is

$$H(f) = \frac{1}{1 + (jf/f_{3\text{dB}})}.$$

Thus, the filter has 3-dB frequency $f_{3\text{dB}}$ and filter time constant $\tau = \frac{1}{2}\pi f_{3\text{dB}}$. Its response to a rectangular pulse is piecewise exponential in form. We agree to base our decision on the output of this filter at the end of the bit. The problem is to optimize the trade-off between achieving large signal response (obtained with wide bandwidth) and minimizing noise power (with narrow bandwidth). Give an expression for the SNR at the sampling instant, $\text{SNR} = \mu^2/\sigma^2$, and maximize with respect to $f_{3\text{dB}}$. Also, calculate the resulting loss in SNR relative to the optimal detector. You should find the loss is on the order of 1 dB, which is not too disappointing, given the filter's simplicity. However, the performance is further degraded when we consider synchronous transmission because the filter retains a residual influence from previous symbols.

3.3.7. Three different eight-point constellations are proposed as shown in Figure P3.3.7. Draw the appropriate decision boundaries for each technique in two dimensions, and express P_s in terms of *peak* energy-to-noise density ratio. Repeat for an *average* energy normalization. Which of the demodulators would be easier to implement?

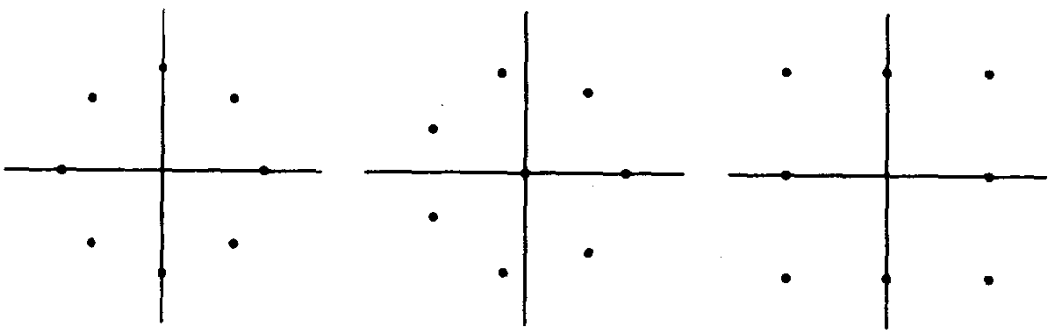

Figure P3.3.7

3.3.8. Construct the 3-ary simplex design as follows. Begin with a 3-ary orthogonal signal space, and from each signal vector, subtract the center of mass of the original constellation. What is the energy in each of the new signals? Show that the normalized inner product between signals is $-\frac{1}{2}$. Finally, show that the three signals can be described by a two-dimensional

basis and that the signal space may be recast as vertices of an equilateral triangle in two-dimensional space, or as 3-PSK.

3.3.9. We will consider a simple argument regarding the asymptotic performance of orthogonal signaling. Suppose that the communication channel can supply a received power level of P_r watts, with a noise level of $N_0/2$ W/Hz.

(a) First, argue that with orthogonal signaling the probability of confusing any transmitted signal for any one of the alternatives is bounded by

$$P_2 = \frac{1}{2}e^{-E_s/2N_0}.$$

(This is an upper bound for coherent detection, but exact for noncoherent detection, as shown in Section 3.4.)

(b) Now apply a simple union bound to show that the probability of symbol error is bounded by

$$P_s \leq (M-1)P_2 < MP_2 = e^{\log_e M} e^{-E_s/2N_0}.$$

(c) Now recall that $E_s = \log_2 M E_b$ to obtain the result that

$$P_s < \exp\left[\log_e M\left(1 - \frac{E_b}{N_0}\frac{1}{2\log_e 2}\right)\right]$$

and hence the result that as M becomes large the symbol error probability can be made arbitrarily small provided $E_b/N_0 \geq 2\log_e 2 = 1.4$ dB.

3.3.10. Biorthogonal signaling with $M = 32$ was utilized as an efficient modulation scheme for NASA's Mariner 1969 space probe. The construction of the signal set was based on Hadamard matrices, as described in Example 3.6. The baseband Hadamard pulse sequence phase-modulated a microwave carrier near 2.3 GHz.

(a) Show how a coherent receiver can be implemented that uses only one radio-frequency correlation, followed by baseband processing. In particular, show how we can integrate over each chip interval, producing real variables, which can become inputs to a "digital correlator." The latter box is really a system for performing signed addition according to the rows of the Hadamard matrix and amounts to performing the Hadamard transform of the received 16-dimensional vector.

(b) Evaluate the symbol error probability when $E_b/N_0 = 5$ dB.

(c) If the output of the Hadamard sequence generator is modeled as an independent binary sequence, except that the rate is scaled accordingly, determine the width of the power spectral density (main lobe) assuming an information rate of 10 kbps.

3.3.11. Show that, by subtracting from each signal point of an M-ary orthogonal construction a vector corresponding to the center of mass, the resulting constellation has energy $E_{\bar{s}} = E_s(M-1)/M$.

3.3.12. Verify that the signal set formed by the seven cyclic shifts of 1, 1, 1, −1, −1, 1, −1, a length 7 pseudorandom sequence, augmented with an eighth signal −1, −1, −1, −1, −1, −1, −1, forms an 8-ary simplex. To do so requires showing that the normalized inner product between signal-space vectors is $-\frac{1}{7}$. Describe two different seven-dimensional bases for this set of signals. Find P_s for the AWGN channel when $E_b/N_0 = 8$ dB.

3.3.13. Graph P_s for the differential encoding/decoding of 4-PSK, with coherent detection, as a function of E_b/N_0. Determine the increase in required E_b/N_0 at $P_s = 10^{-5}$ over regular 4-PSK.

3.3.14. Evaluate P_s for 32-QAM as described in Section 3.3.5 and determine the E_b/N_0 needed to achieve $P_s = 10^{-5}$. Determine the ratio of peak signal energy to average signal energy

for this modulation scheme. Experiment with bit labeling schemes that minimize bit error probability.

3.3.15. In digital microwave radio, the quest for spectrum efficiency has spawned equipment that now uses 256-point QAM transmission. Determine the E_b/N_0 necessary to achieve a bit error probability of 10^{-7}, assuming a square constellation. Use upper bounds for the Q-function from Chapter 2.

3.3.16. Show that 16-QAM can be synthesized by the use of two QPSK modulators in parallel, as shown in Figure P3.3.16, with one of the modulator outputs attenuated by 6 dB, or a factor of one-half in amplitude. This technique is referred to as superposed modulation and allows high-power-level modulation to be performed without the need for linear amplitude modulators/amplifiers. Generalize the approach to the synthesis of 64-QAM.

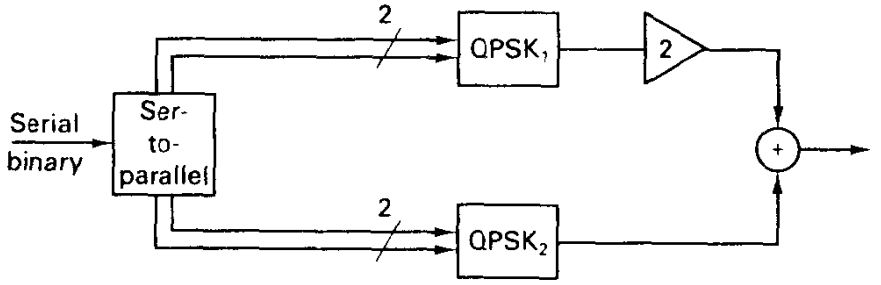

Figure P3.3.16

3.3.17. The 16-point constellation adopted in the V.29 standard for 9600-bps voice-band modems is shown in Figure P3.3.17.

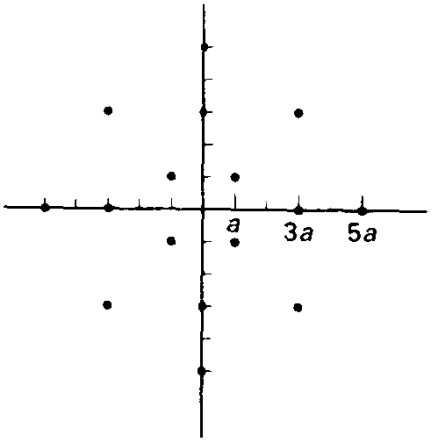

Figure P3.3.17

(a) Draw decision zones for the AWGN channel. (They are not as simple as in the rectangular 16-QAM design.)

(b) Calculate the average energy of the signal set in terms of a, and determine upper and lower bounds on P_e. Note that each signal point does not have the same set of nearest neighbors. You should determine that this constellation is less energy efficient than the standard 16-QAM design.

(c) One advantage of this constellation is a smaller degradation under carrier phase error in the demodulation, which causes a rotation of signal space relative to the decision boundaries. Discuss qualitatively the effect for the V.29 and standard 16-point designs.

3.3.18. Design a 64-point constellation formed from the D_4 lattice as follows. Offset the D_4 as lattice by adding the vector (1/2, 0, 1/2, 0) to every lattice point, or equivalently shift the origin by the same amount.

(a) Show that the innermost two shells plus a portion of the third shell includes exactly 64 points, and find the average energy per symbol, normalized to the minimum squared distance between points.

(b) Show that $E_s = 3.375$

(c) Evaluate an upper bound on P_s by realizing that in the worst case a point in the constellation has 24 nearest neighbors.

(d) Compare this bound with that for 8-PSK, a choice that would have the same signal-space dimensionality per bit transmitted, and determine the relative energy efficiency afforded by four-dimensional signaling.

(e) Describe how such a signal set may be realized using two consecutive signal intervals of two-dimensional QAM-type modulation.

3.3.19. Conway and Sloane discuss so-called Voronoi codes in [22], and produce the 16-point design drawn from A_2 shown in Figure P3.3.19.

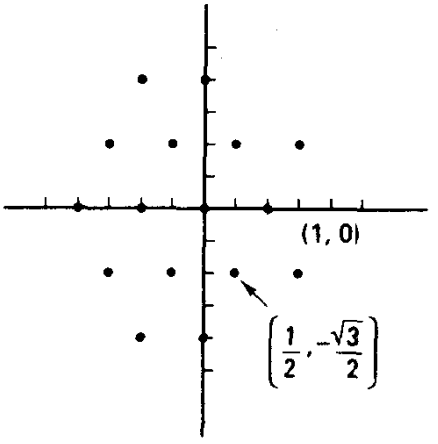

Figure P3.3.19

(a) Calculate the ratio $d_{\min}^2/\overline{E_s}$.

(b) Calculate an upper bound on P_s, and compare with the result for (square) 16-QAM.

3.3.20. Suppose we employ antipodal NRZ signals of duration T on a nonideal channel whose impulse response is a rectangular pulse of duration αT, $\alpha < 1$. Apply matched filter theory to determine the optimal one-shot receiver structure and the resulting *matched filter bound* for performance on this dispersive channel. This involves calculating the energy in the distorted difference signal.

3.3.21. Consider transmission of a single bit using bipolar rectangular pulses with duration T. Let these be passed through a linear channel having impulse response given by

$$h(t) = \frac{1}{\tau}[u(t) - u(t - \tau)],$$

which is a low-pass channel having unity gain at zero frequency. Suppose the signal is received in the presence of white Gaussian noise. Determine the shape of the distorted signals at the receiver, and thus describe the impulse response of the optimal single-symbol detector. Find the energy in the filtered difference signal, E_d', and evaluate the loss in detection efficiency implied by the matched filter bound as a function of τ/T.

3.4.1. Consider baseband 8-ary orthogonal signaling using the Hadamard matrix of order 8.

(a) Using a basis-function receiver with eight nonoverlapping rectangular pulses, show how a single time-shared integrator followed by a digital correlator can implement the optimal receiver. This correlator, if implemented using straightforward vector multiplications, would require $8(8) = 64$ addition/subtraction operations per modulator symbol. A fast Walsh–Hadamard transform, analogous to the fast Fourier transform, can compute all the correlations in $8 \log_2 8 = 24$ addition/subtraction operations, however.

(b) If the Hadamard "chips" PSK modulate a carrier, show how to optimally detect the signals; in particular, note that we should not decide the sign of each chip and then do some sort of logical operation on these.

(c) With modulation as in part (b), show how to perform noncoherent detection.

(d) Evaluate P_s for both coherent and noncoherent detection when $E_b/N_0 = 7$ dB.

(e) If receiver phase coherence is possible, show how to design an 8-ary biorthogonal set with half the dimensionality and slightly better error performance.

3.4.2. One realization of orthogonal signaling uses M-ary FSK, in which the modulator produces a sinusoid at frequency $f_i = f_0 + i\Delta f, i = 0, 1, \ldots, M - 1$. Suppose that the frequency spacing is equal to the symbol rate R_s. An implementation of a noncoherent receiver is a matched filter bank followed by envelope detectors. The matched filters are centered at the respective frequencies. Show that an alternative implementation is possible that samples the received signal at an appropriate rate, computes a discrete Fourier transform DFT at the respective frequencies, and decides in favor of the channel having the largest DFT magnitude (or magnitude squared).

3.4.3. Derive the result that for noncoherent detection of binary on–off keying (OOK) the bit error probability may be approximated by, for high SNR,

$$P_b \approx \frac{1}{2} e^{-E_b/4N_0}.$$

Hint: The output of the noncoherent matched filter is either Rayleigh distributed, in the case of no signal, or Rician distributed, in the case of signal present. The optimal threshold should be set at the intersection of the two conditional p.d.f.'s, but a reasonable approximation is to assume that this point is $\mu/2$, where μ is the detector output magnitude with signal present, but without noise. By integrating the p.d.f.'s over appropriate error regions and by making a Gaussian approximation (mean μ) to the Rician density, you should be able to demonstrate the above for large SNR. Here one error type dominates the other at large SNR.

3.4.4. In pulse compression radar, a phase-coded RF pulse is transmitted at the target and is received at a later time with total energy E_s in the presence of white Gaussian noise. Let the baseband pulse be defined by the seven-chip sequence with polarity pattern $+ + + - - + -$, with each chip lasting $T_s/7$ seconds. The receiver cannot determine the return signal phase and so performs noncoherent detection. Diagram the structure of the optimal receiver, and show the response of the envelope detector output when excited by the signal. The output pulse has the same shape as the signal autocorrelation function, which is narrow in time, leading to accurate range measurement. (The radar problem differs from the digital communications framework in that the sampling time is not known a priori—radar receivers merely place an amplitude threshold on the output of the detector to declare presence of target.)

3.4.5. Demonstrate that to maintain orthogonality the frequency spacing between FSK signals that are phase coherent is $\Delta f = mR_s/4$, while for noncoherent FSK signals (derived from different oscillators perhaps), the spacing must be $\Delta f = mR_s/2$.

3.4.6. An optical communication system utilizes 256-ary pulse-position modulation of a laser to send messages. This provides an orthogonal signal set. At the output of the photodetector

in the receiver, we model the resulting photocurrent as the sum of the transmitted signal plus an additive white Gaussian noise (here called shot noise arising in the detection process). If the mean detector output is A amperes during presence of a pulse, and the additive noise has power spectral density $N_0/2$ A^2/Hz, give an expression for bit error probability.

3.5.1. In 4-ary DPSK, the receiver measures the following sequence of phases: 79°, 95°, 51°, 235°, 219°, 38°. Decode the sequence using the first phase measurement as a reference.

3.5.2. In PSK or DPSK reception, the receiver first estimates the phase of the signal in the nth interval as shown in Figures 3.3.20 and 3.5.1. [It may be shown that

$$\gamma_n = \tan^{-1}\left(\frac{r_{s_n}}{r_{c_n}}\right)$$

is a maximum likelihood estimate of phase angle, given no prior information about the angle.] Without loss of generality, assume that the true phase angle is zero so that

$$\gamma = \tan^{-1}\left(\frac{n_s}{A + n_c}\right)$$

is the phase error, with n_c and n_s denoting the in-phase and quadrature components of the noise.

(a) By invoking a large-SNR approximation and a small-angle approximation, show that the phase error is zero-mean Gaussian with variance $\sigma^2 = N_0/2A^2$, as SNR becomes large.

(b) Determine under these same approximations the distribution for the phase difference of two consecutive measurements, as performed in DPSK.

3.5.3. Show that implementation of the 4-ary DPSK decision can be implemented by forming both the vector inner product and vector cross product of successive phasor measurements and then comparing each with zero thresholds. This will determine in what quadrant the measured phase difference lies. Diagram a receiver.

3.5.4. A communication link can supply $P_r = 10^{-12}$ W of signal power, with the noise level at the same point in the receiver measured to be $N_0/2 = 10^{-20}$ W/Hz. The desired bit error probability is $P_b = 10^{-5}$. What are the achievable bit rates with the following options?

(a) Coherent PSK

(b) 4-ary orthogonal signals, coherent detection

(c) 8-PSK

(d) 8-DPSK

For implementation losses in the demodulator due to synchronization and the like, allow a 1-dB inefficiency relative to theoretical performance.

3.5.5. Computer simulation is a frequent means of evaluating digital system performance, especially in cases where nonlinearities, filtering, and/or non-Gaussian noise may be present. This exercise introduces the art.

(a) Let's consider simulation of 8-PSK modulation. We often do not need to simulate the waveform aspects of the problem, but produce instead random variables with appropriate densities. The basis function receiver would, under assumption of the S_0 message being transmitted, produce for r_0 a Gaussian random variable with mean $E_s^{1/2}$ and variance $N_0/2$. On the other hand, r_1 would be zero-mean Gaussian with the same variance.

(b) Generate pairs of independent Gaussian variables using the Box–Muller method:

$$Z_0 = (-2\log_e U_1)^{1/2}\cos(2\pi U_2).$$

$$Z_1 = (-2\log_e U_1)^{1/2}\sin(2\pi U_2).$$

where U_1, U_2 are independent variables uniformly distributed on [0, 1) and commonly available from random number generators. To Z_0, add a constant to provide the proper mean.

(c) Perform a decision by deciding whether the measurement is inside the pie-shaped sector $\pi/8$ radians on either side of zero. Count the number of errors in 1000 trials, when $E_b/N_0 = 10$ dB. Do you agree with the theoretical result? (In 1000 Bernoulli trials, the standard deviation of the measured mean is $[P_s(1 - P_s)/1000]^{1/2}$.) Remember to scale energy properly.

3.6.1. What average E_b/N_0 is required to produce $P_s = 10^{-3}$ for the following options on the Rayleigh slow-fading channel?

(a) Coherent binary PSK

(b) Binary DPSK

(c) 8-ary orthogonal (FSK) with noncoherent detection

(d) 8-ary DPSK

Repeat for $P_s = 10^{-5}$.

3.6.2. Other popular fading models are the Rician and log-normal models. In Rician fading, $A(t)$ has a p.d.f. given by

$$f_A(a) = \frac{a}{\sigma^2} I_0\left(\frac{\mu a}{\sigma^2}\right) e^{-(a^2+\mu^2)/2\sigma^2}, \qquad a \geq 0.$$

In log-normal fading, so named because the logarithm of the amplitude is held to be normally distributed,

$$f_A(a) = K e^{(\log_e a - \mu)^2/2\sigma^2}.$$

(a) Plot p.d.f.'s for both when $\mu = 3$ and $\sigma = 1$.

(b) Formulate integral expressions that could be integrated to compute symbol error probability for DPSK transmission over such a channel, assuming the fading is slow.

3.6.3. Generate a Rayleigh random process in discrete time using a computer random number generator to produce two independent Gaussian variates as in Exercise 3.5.5; then compute the root sum square of these. To make the process have a desired correlation time, or bandwidth, the Gaussian sequences should be generated by filtering white Gaussian sequences in each case with identical low-pass filters. If you wish to simulate a case where the ratio of symbol rate to fading bandwidth is 100, constituting a slow-fading case, the difference equation

$$Y_n = 1.94Y_{n-1} - 0.95Y_{n-2} + W_n - 1.94W_{n-1} + W_{n-2}$$

will suffice. This is a two-pole elliptic filter with rather sharp transition from passband to stopband. It is instructive to view time-domain plots, amplitude histograms, and spectra of the complex Gaussian random sequence using an FFT routine.

3.6.4. Sometimes the figure of merit for channels is not the average error probability, but the outage probability, defined as the probability (percentage of time) that the link has an error probability greater than some acceptable level, say 10^{-4}. Suppose we have a Rayleigh fading channel and wish an outage probability less than 1%. Use the Markov inequality to see where to design the nominal link operating point if DPSK transmission is utilized. (*Answer*: The average SNR must be set 13 dB higher than that required to give 10^{-4} performance, to allow for the fading.)

3.7.1. *Consider binary baseband signaling with*

$$s_0(t) = -A\phi_0(t), \qquad s_1(t) = A\phi_0(t),$$

and

$$\phi_0(t) = (2/T_s)^{1/2} \sin^2\left(\frac{\pi t}{T_s}\right),$$

as shown in Figure P3.7.1. Show that the power spectrum is

$$G_s(f) = K \frac{\sin^2(\pi f T_s)}{(fT_s)^2 [f - (1/T_s)]^2 [f + (1/T_s)]^2}.$$

Furthermore, show that the first null in the spectrum is at $f = 2R_s$, and nulls occur at every multiple of the symbol rate thereafter. Notice also that for large frequency the rate of decay of spectral sidelobes is $O(f^{-6})$.

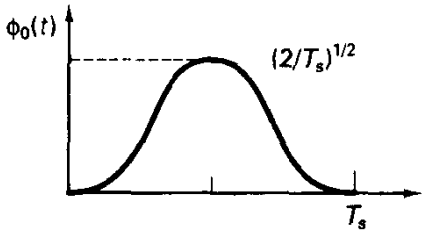

Figure P3.7.1

3.7.2. RZ (return to zero) signaling uses the two signals shown in Figure P3.7.2. Determine the baseband power spectrum for this transmission strategy. At what frequencies do spectral lines exist?

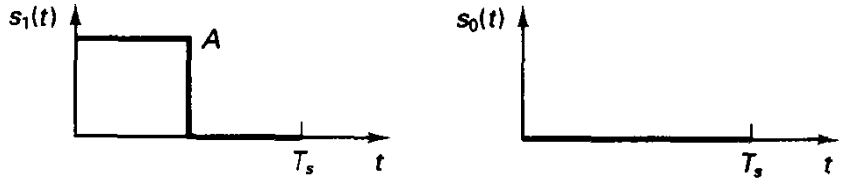

Figure P3.7.2

3.7.3. Determine the power spectral density for 4-PSK and 8-PSK transmission options for a satellite link when the bit rate is 140 Mbps. Assume that the carrier frequency is f_c = 6.0 GHz and that a NRZ pulse shape is used. Repeat if square-root, raised-cosine shaping, with excess bandwidth factor 0.25, is used. Which option makes the most sense if the nominal transponder bandwidth is 72 MHz?

3.7.4. Data transmission over the dial-up voiceband network is accomplished in various formats and data rates. One technique utilizes 16-QAM signaling on a 1800-Hz carrier to achieve 9600 bps throughput. The symbol rate is therefore 2400 Hz. Instead of rectangular pulse shaping, suppose we use a raised-cosine pulse shape having an excess bandwidth factor of 0.2. What is the resultant power spectrum? In particular, show that the spectrum is zero outside of (360 Hz, 3240 Hz).

3.7.5. Adopt 8-ary PPM as a baseband transmission format, and use the generic expression for the power spectral density to determine $G_s(f)$. Simplify as much as possible. Are spectral lines

present? Write a short computer program to evaluate the power spectrum, and give a rough assessment of bandwidth. What happens when we shift to 16-ary PPM with the *same* bit rate?

3.7.6. Consider binary FSK wherein the transmitted signal switches between two oscillators according to the message bit to be sent. Thus, the signals are defined by

$$s_0(t) = A\cos(2\pi f_0 t + \Theta_0)$$

and

$$s_1(t) = A\cos(2\pi f_1 t + \Theta_1)$$

for a duration T_b seconds. Here the phase angles are defined to be independent random variables, uniformly distributed on $[0, 2\pi)$. A representation for the aggregate signal over time is

$$s(t) = \frac{1 + d(t)}{2}\cos(2\pi f_0 t + \Theta_0) + \frac{1 - d(t)}{2}\cos(2\pi f_1 t + \Theta_1),$$

where $d(t)$ is the unit-amplitude random binary wave discussed in Chapter 2.

(a) Show that the autocorrelation function for this signal is

$$R_s(\tau) = \frac{A^2}{8}[(1 + R_d(\tau))\cos(2\pi f_0\tau) + (1 + R_d(\tau))\cos(2\pi f_1\tau)],$$

where $R_d(\tau)$ is the (triangular) autocorrelation function of the unit-amplitude random binary wave having bit rate $1/T_b$.

(b) Show then that the power spectrum is comprised of two spectral lines at the respective oscillator frequencies, plus two sinc-squared lobes centered at each frequency, with bandwidth corresponding to NRZ modulation of each carrier. This result holds for any choice of f_0, f_1. The spectrum is somewhat different, however, if the modulation is achieved by frequency-modulating a single oscillator, which enforces a phase continuity condition.

(c) Plot the power spectrum for the cases $f_0 = 1070$ Hz and $f_1 = 1270$ Hz, with $R_b = 300$ Hz (corresponding to a 300-bps FSK data modem).

3.7.7. Derive the same result for the power spectrum in Exercise 3.7.6 by defining the complex envelope of each signal relative to the frequency midway between the two oscillator frequencies and then finding the baseband power spectrum as discussed in the text; then, finally, apply frequency shifting to the carrier frequency.

3.7.8. The IEEE 802.4 token-passing local area network protocol uses an FSK system for binary data transmission, with the two signals shown in Figure P3.7.8. Either one or two cycles of a sinusoidal carrier is sent per bit interval. Determine the power spectral density of the modulator output signal.

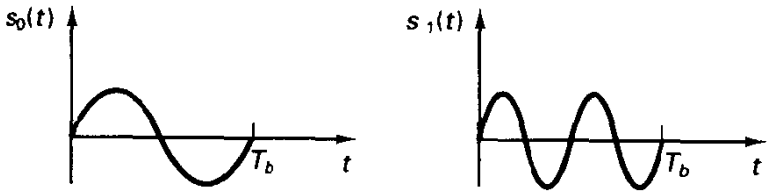

Figure P3.7.8

3.8.1. Diagram a maximal length sequence generator for a 15-bit sequence, using the feedback connections supplied in Figure 3.8.2, and list one period of the sequence. By representing the sequence in ± 1 format, compute the autocorrelation function of the sequence by integrating

the product of the sequence and a delayed version over one period. Verify the result is as shown in Figure 3.8.2c.

3.8.2. The family of Gold sequences is obtained by taking two preferred maximal-length sequences of equal period and modulo-2 adding their outputs to produce another binary sequence with the same period. If we phase shift one sequence relative to the other, still another binary sequence is obtained. Consider length-15 sequences, and let one constituent be the sequence formed in Exercise 3.8.1. Let the other be the sequence formed by feeding back the modulo-2 sum of bits 3 and 4 in a four-bit shift register. (This is another maximal-length sequence.) Form the Gold code obtained by starting both generators in the all 1's state. List its sequence of bits, and determine the cyclic autocorrelation of this sequence with itself. If you wish to pursue this further, form another Gold sequence by shifting either constituent sequence by one chip, and perform a cross-correlation analysis of the two Gold sequences.

3.8.3. For a DS system with 255 code chips per information bit, calculate the processing gain in decibels, and determine the error probability for PSK signaling with $E_b/N_0 = 10$ dB and a tone interferer with 5-dB larger power at the receiver. Does additive noise or interference dominate the error probability calculation?

3.8.4. Derive the optimal combining rule for combining the receiver outputs with H hops per bit, assuming noncoherent detection on each hop and independence of phases from hop to hop. In particular justify (3.8.14). *Hint*: Write the likelihood function for the two cases, assuming independent channel action on each hop, with Rician or Rayleigh p.d.f.'s; then take logarithms and eliminate common terms.

3.8.5. Consider a partial-band noise jammer with fill factor ρ and fast frequency hopping with H hops per bit. Suppose that the modulation is binary FSK, with noncoherent detection, and that the receiver has side information on whether a given hop is jammed by noise or not. Show that

$$P_b = \rho^H P(\text{error for } H \text{ hop combining} | N_{0_J})$$

Use the expression derived in Section 3.8 for the error probability with fast hopping, and retain only the leading term of the expansion to substitute in this expression. Determine from this the worst-case ρ, and show that for large E_b/N_{0_J} the error probability expression has slope $-H$.

3.8.6. Consider a fast-hopping system with binary FSK modulation. Instead of performing optimal combining as in (3.8.14), we may elect to perform binary decisions on each hop and decide finally based on majority vote. (This is particularly attractive if the receiver does not know which hops have been jammed and thus cannot form optimal combining rules.) Formulate the expression for final error probability, and show that with a worst-case jammer the slope of the error probability curve is $-(H-1)/2$ for H odd.

3.8.7. Plot the conditional p.d.f.'s given in the text for the fast frequency-hopping case when $E_b/N_0 = 10$ dB and $H = 5$.

3.8.8. Repeat the calculations of Example 3.20 when the modulation is binary DPSK. Determine the worst-case ρ and the resulting expression for error probability. Assume sufficiently slow hopping that the DPSK overhead is negligible.

3.8.9. Suppose in a CDMA system employing DS spread spectrum that two users transmit simultaneously and that the codes possess 127 chips per bit. Due to delay differences, assume that the worst-case cross-correlation occurs when 66 chips agree and 61 differ. Calculate the normalized cross-correlation and the decision SNR if $E_b/N_0 = 10$ dB and $\gamma = 1$. Assume that all sources of impairment can be modeled as Gaussian at the detector output and that variances add.